BILINGUAL PUBLISHING CO.
Pioneer of Global Academics Since 1984

Organic Polymer Material Research

Volume 4 | Issue 2 | December 2022 | ISSN 2661-3875（Online）

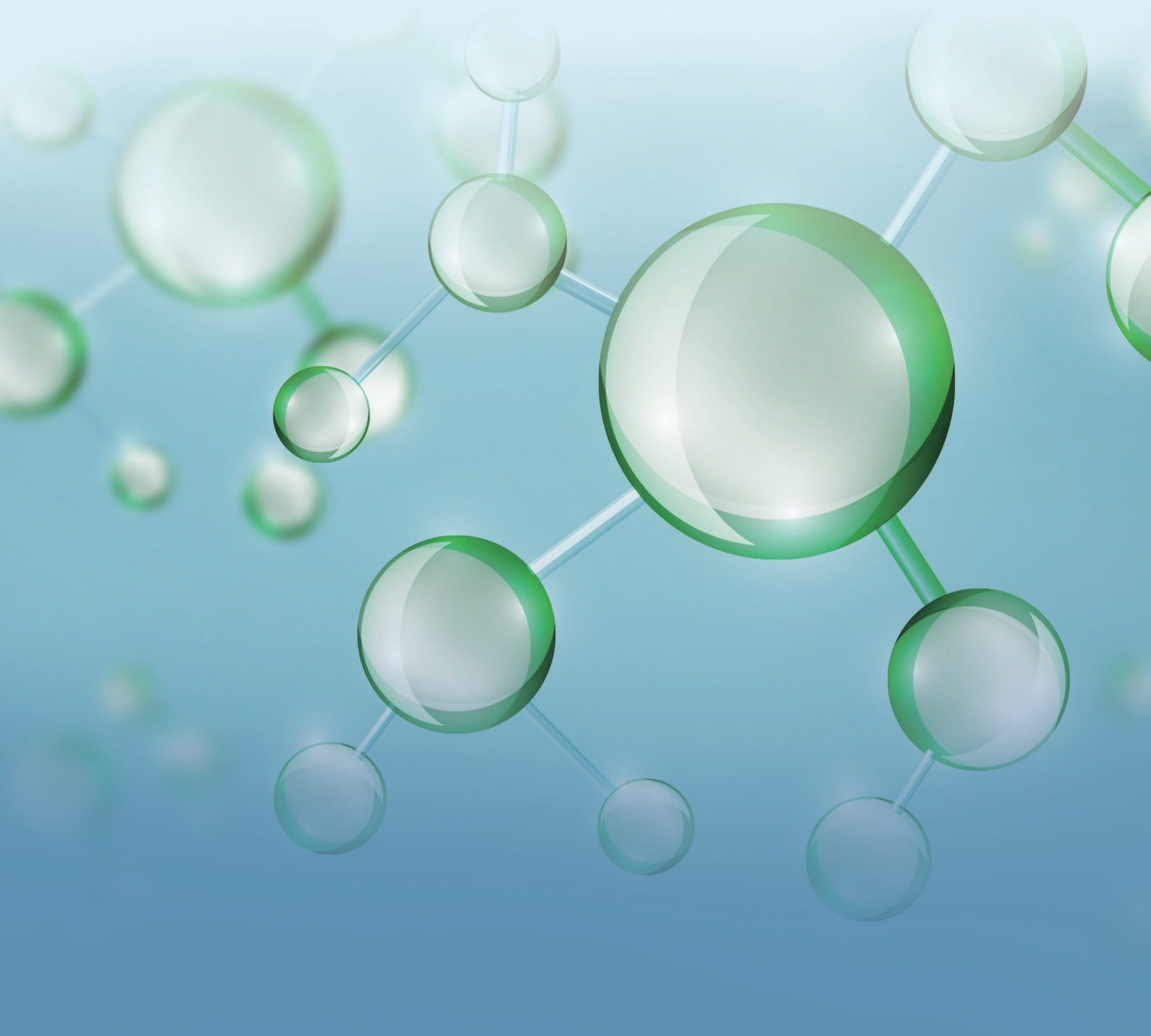

Volume 4 Issue 2 • December 2022 • ISSN 2661-3875 (Online)

Organic Polymer Material Research

BILINGUAL PUBLISHING CO.
Pioneer of Global Academics Since 1984

BILINGUAL PUBLISHING CO.
Pioneer of Global Academics Since 1984

Volume 4 | Issue 2 | December 2022 | Page1-25
Organic Polymer Material Research

Contents

Articles

BILINGUAL PUBLISHING CO.
Pioneer of Global Academics Since 1984

Organic Polymer Material Research
https://ojs.bilpublishing.com/index.php/opmr

ARTICLE

N-heterocyclic Carbene Catalysed Polymerisation of 2,5-Diformylfuran

Wouter Ruelens[1] Fariba Mafakheri[1,2] Viktor Van Lierde[1] Mario Smet[1*]

1. Department of Chemistry, KU Leuven, Leuven, 3001, Belgium
2. Department of Polymer Chemistry, School of Chemistry, College of Science, University of Tehran, 14155-6455, Iran

ARTICLE INFO

Article history
Received: 11 August 2022
Revised: 08 October 2022
Accepted: 18 October 2022
Published Online: 11 November 2022

Keywords:
Biobased polymer
2,5-diformylfuran
NHC

ABSTRACT

The biobased renewable monomer 2,5-diformylfuran is polymerised using various N-heterocyclic carbene (NHC) catalysts in dimethyl sulfoxide (DMSO) affording a low molar mass polymer. It is shown that catalyst structure as well as the temperature and time the polymerization is running have a noticeable effect on its molar mass. The obtained material is characterized by nuclear magnetic resonance (NMR), thermogravimetric analysis (TGA), differential scanning calorimetry (DSC) and X-ray diffraction (XRD). An attempt at chain extension with diamine leads to precipitation of the polymer. This new biobased polymer material might be useful as a sustainable resin.

1. Introduction

As society is becoming more aware of its impact on the environment, there is an increasing motivation to move away from fossil resources. This poses a great challenge for the development of new chemical processes as almost all of the current industrial processes rely heavily on petroleum resources. As it is undesirable for this new feedstock to interfere with the production of food, as well as for economic reasons, this feedstock would preferably originate from agricultural waste streams. These waste streams consist mainly of cellulose, hemicellulose and lignin [1-3]. In order to be able to produce high purity chemicals these polymers have to be broken down into smaller chemicals enabling fractionation and purification. In case of the polysaccharides cellulose and hemicellulose this can be easily achieved by combined acid hydrolysis and dehydration producing 5-hydroxymethylfurfural (HMF) and furfural, respectively [2,4-7]. For the case of lignin this can be achieved by oxidation to vanillin derivatives or by hydrogenolysis to phenols and various other aromatics [3,8-10].

Due to the significantly higher yields and easier purification, the furans are currently more appealing from an industrial point of view [4,11]. Furfural is mainly hydrogenated towards furfuryl alcohol and subsequently polymerized

**Corresponding Author:*
Mario Smet,
Department of Chemistry, KU Leuven, Leuven, 3001, Belgium;
Email: mario.smet@kuleuven.be

DOI: https://doi.org/10.30564/opmr.v4i2.4953

to poly(furfuryl alcohol) resins, which find applications in the foundry industry as well as wood preservation [4]. HMF, however, has a wider range of applications. It can be reduced to produce fuels and fuel additives such as 2,5-dimethylfuran, dodecane… [3,5]. When oxidized, however, 2,5-diformylfuran (DFF) and 2,5-furan-dicarboxylic acid (FDCA) can be synthesized. The latter has gained a lot of attention as it could be used as a biobased alternative for terephthalic acid in polyester production [12,13]. DFF has also been used for the synthesis of various polymers such as polyimides [14,15], polypinacols [16], urea resins [17]… Our work focuses on the benzoin coupling for the polymerisation reaction. The analogous polymer bearing benzene rings instead of furan, polybenzoin, has been reported in literature, but to the best of our knowledge the furan analogue, polyfuroin, has not [18,19].

The benzoin coupling is a C-C coupling reaction transforming two aldehydes into an α-hydroxy ketone. During the reaction a nucleophilic catalyst adds to one of the aldehydes transforming it into a nucleophile itself. This newly formed nucleophile will then add to the other aldehyde after which the catalyst is eliminated. When the reaction was first discovered, a cyanide catalyst was used [20]. Later it was found that the same reaction could be catalysed by thiazolium species in the presence of base, in a biomimetic reaction [21]. This was then expanded towards a broad range of N-heterocyclic carbenes (NHC), which have proven to afford higher yields and to be less toxic [22]. Another advantage of the use of NHC's instead of cyanide is that they can be produced enantiomerically pure allowing for stereocontrol of the reaction products.

2. Materials and Methods

2.1 Instrumentation and Measurements

^{1}H-NMR measurements were performed in DMSO-d6 using a Bruker Avance 400 operating at 400 MHz. DSC measurements were done on a TA instruments Q2000 with heating/cooling rates of 10 K/min and isothermal segments of 5 min at the temperature limits. TGA measurements were carried out using a TA instruments Q500 with a heating rate of 10 K/min to 550 °C in nitrogen.

2.2 Synthesis of NHC Precatalysts

Precatalysts **1'** (Figure 1) were made according to literature with exception of the respective hydrazine used [23]. Purification of these precatalysts could either be achieved by recrystallisation from methanol (**1'a**) or by column chromatography, which produced both pure **1'** as **1**. Precatalyst **1a** was made by deprotection of **1'a** with TMSBr in methanol according to literature [23].

Precatalysts **2** were also synthesised according to literature procedures [24]. The procedures were modified with the appropriate hydrazine derivative for synthesising the required precatalyst structure.

Precatalysts **3** were also produced according to literature procedures [25]. For catalyst **3a** the perchlorate was not purified, but the methanol adduct was synthesised instead. This was not feasible for the other derivatives due to them not forming a precipitate.

Precatalysts **4** and **5** were synthesised according to literature procedures [26].

To the best of our knowledge the synthesis of precatalysts **1'b**, **1d** and **3b** has not yet been reported in literature. Therefore more detailed synthesis procedures and characterization data of these compounds and ^{1}H NMR data of the other precatalysts are added in the supplementary information.

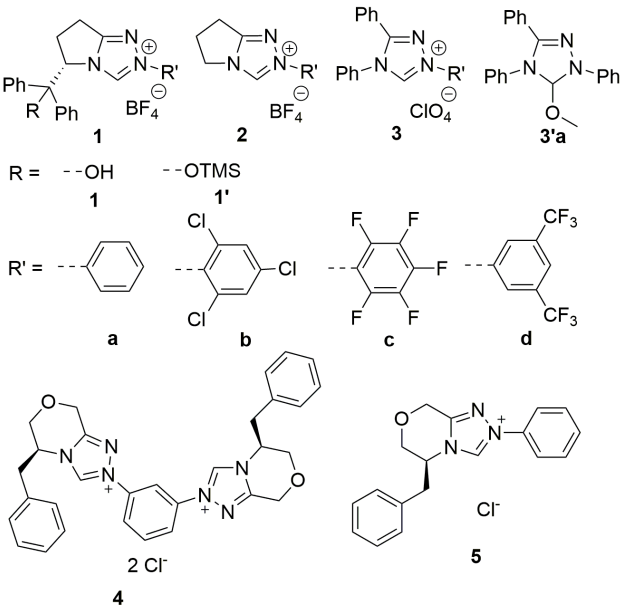

Figure 1. Structures of the NHC precatalysts

2.3 Synthesis of Polyfuroin

A dry Schlenk tube was charged with a stirring bar, 2,5-diformylfuran [7,27] (248 mg; 2.00 mmol) and NHC precatalyst (0.04 mmol). Three cycles of vacuum-inert gas were applied to the tube and its contents. Subsequently 3 mL of dry, degassed DMSO were added to the tube and it was heated to 40 °C. To start the reaction dry, degassed triethylamine (0.13 mL; 1.0 mmol) was added to the reaction mixture and it was left to stir for 24 h. The reaction was quenched by the addition of a small amount of methanol and subsequently precipitated in 50 mL of 1 mM aqueous HCl. The precipitate was filtered and washed with water before being dried in a vacuum oven at 40 °C.

When catalyst **3'a** was used, the catalyst was placed under vacuum for 24 h at 90 °C. Afterwards nitrogen was let into the tube and it was left to cool to the reaction temperature after which the monomer solution was added to the catalyst.

2.4 Imine Coupling

The (pre-)polymer was dissolved in DMSO. When it was fully dissolved a stoichiometrical amount of diamine was added. This mixture was left to stir at room temperature for 1 h. Afterwards the polymer was precipitated in water, filtered and dried under vacuum.

3. Results and Discussion

3.1 Polymer Synthesis

For the polymer synthesis the choice of solvent is crucial. When an ethereal solvent like THF or 1,4-dioxane are used the polymer precipitates quickly upon formation of very short oligomers. Tests with the monofunctional furfural also led to precipitation indicating that dimers could already come out of solution in these solvents. The precipitation of the polymer leads to shorter chains as further polymerisation is inhibited. More polar solvents such as DMSO or pyridine were able to keep the polymer in solution. Due to the toxicity of pyridine further experiments were only conducted in DMSO. These results are in contrast to those obtained from the polymerisation of terephtaldehyde, where polymerisation in THF afforded higher Mw than in DMSO [18].

Upon activation of the catalyst by the addition of base, the reaction mixture turns a dark colour (purple-brown). This colour is also present in the final polymer.

From the data in Table 1 it is clear that catalyst type, time and temperature all have an influence on the molar mass of the obtained polymers. Catalysts of the **1'** series slightly outperform the other catalyst structures, but all of them improve when a more electron withdrawing substituent is used on the phenyl ring attached to the nitrogen. Both an increase in the temperature and duration of the polymerisation increase the molar mass of the polymers obtained. The increased molar mass at higher polymerization temperatures could be explained by 2 factors. Either only the increased polymerization kinetics are responsible and the polymerization is stopped closer to its equilibrium or the temperature also affects the equilibrium itself and allows a higher molar mass regardless of polymerization time. The data of longer polymerization times at the same temperature indicate that the polymerization hasn't reached its equilibrium state and the kinetic factor seems more likely, although a shift in equilibrium at higher temperature can't be excluded. What is remarkable, though, is that when the polymerisation is left running for more than 120 h the molar mass decreases again and seems to reach a steady state at around 1500 g/mol.

Table 1. Molar mass and isolated yields of the polymerisations for different catalysts, time and temperature. The polymerisations were carried out in DMSO at a catalyst loading of 2 mol%

Catalyst	Time (h)	Temp (°C)	DPn	Mn (g/mol)	Yield (%)
1a	24	40	3.2	400	75
1'a	24	40	5.6	690	81
1b	24	40	5.6	700	61
1'b	24	40	7.4	920	74
1c	24	40	8.8	1090	77
1d	24	40	30.9	3840	91
2a	24	40	7.1	880	43
2b	24	40	4.3	540	47
2c	24	40	4.4	550	49
3'a	24	40	4.1	510	49
3b	24	40	6.3	790	70
3b	24	50	7.7	950	70
3b	24	60	10.5	1300	71
3b	24	30	5.6	700	68
3b	48	40	12	1490	77
3b	72	40	26.6	3300	77
3b	120	40	36.2	4490	74
3b	144	40	10.9	1310	72
3b	168	40	12.6	1560	78
4	24	40	8.7	1080	75
5	24	40	12	1490	77

3.2 Polymer Characterisation

The first important characteristic is the molar mass of the polymers. Determining this property proved to be a challenge as the polymers only dissolved in viscous highly polar solvents, which were not compatible with our standard columns for SEC (PLgel MIXED). When another column set designed for us with polar solvents was used (PSS Polarsil) adsorption to the column was detected invalidating the results. As an alternative for SEC measurements DOSY measurements were attempted but even at sample concentrations of 10 mg/ml the signal/noise ratio was too low to fit the diffusion coefficient properly and thus no conclusions could be drawn from these measurements. The only remaining option available to us was to estimate the molar mass from concentrated NMR samples via the end-group integration and an assumption of the structure of the polymers. In the ^{1}H NMR spectrum (Figure 2) the signals from the aldehyde end groups can clearly be dis-

tinguished from the other signals. From this the number average degree of polymerisation (DPn) can be calculated, under the assumption that the polymer has no branches and has two aldehyde end groups, by the following formula when the integration of the aldehyde protons is set to two:

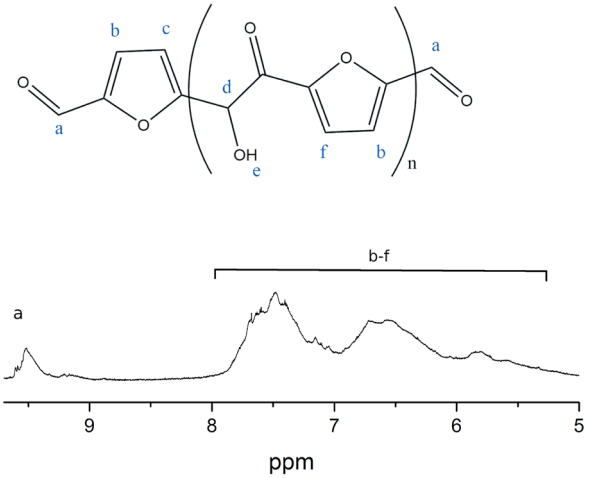

Figure 2. NMR-spectrum of polyfuroin

To assess the thermal stability of the polymer a TGA analysis was carried out under nitrogen atmosphere. The thermogram (Figure 3) shows a small loss of mass already below 100 °C, which can be attributed to the loss of absorbed water. Further loss of mass occurs in two steps each having their highest rate around 260 °C and 430 °C respectively. At the highest temperature of this measurement (550 °C) 51% of the original mass was still left. Visual inspection of the residue shows that it still has the same shape as before the measurement. This suggests that the material does not melt or have a glass transition before thermal degradation sets in.

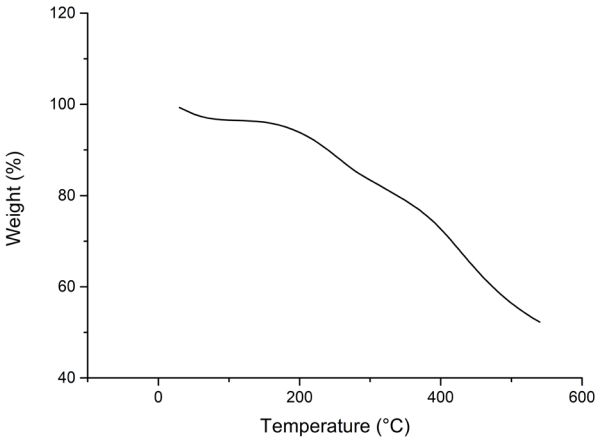

Figure 3. TGA profile of polyfuroin produced using precatalyst 1c

To test this DSC measurements were carried out on the polymer. In the entire thermogram no transition of any kind is visible supporting the hypothesis that the polymer degrades before any thermal transition (Figure 4). This is further supported by the reported values for the Tg of the similar polybenzoin between 112 °C and 150 °C, which are higher than the degradation point found for this polymer [18].

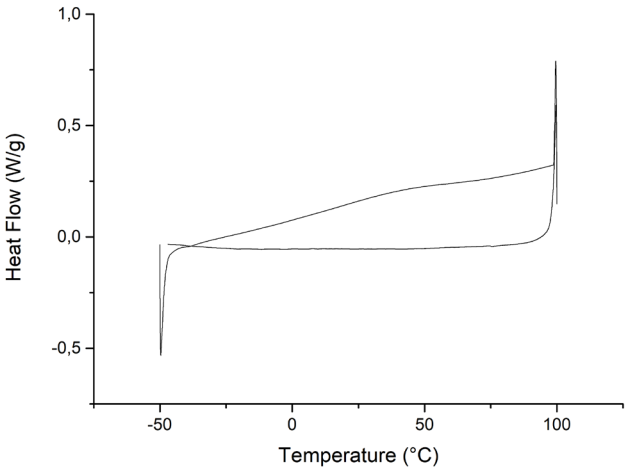

Figure 4. DSC profile of polyfuroin produced using precatalyst 1c. The second heating and cooling cycles are shown.

As the low degradation temperature made it impossible to check the crystallinity by thermal measurements, X-ray diffraction experiments were carried out. The main reason for these experiments is to test the hypothesis that the homochiral catalysts can induce sufficient optical homogeneity in the polymer to allow crystallisation. The diffractogram of all polymers, however, did not show any distinct peaks indicating that the material was completely amorphous.

3.3 Imine Coupling of Polyfuroin

When a stoichiometric amount of 1,6-hexamethylenediamine was added to a solution of polyfuroin in DMSO in an attempt to increase its molar mass, a precipitate was formed. This precipitate couldn't be dissolved in either acetone, THF, chloroform, DMSO or DMF. To check if this was an effect of imine coupling of the aldehyde end groups of the polymer, a test reaction was done with DFF instead of polyfuroin at room temperature. This reaction also afforded a precipitate within a few minutes. After workup this polymer was brought into an acidic aqueous solution to hydrolyse the imine and after addition of an organic solvent to dissolve the DFF everything returned back into solution, indicating imine couplings were most likely responsible for the precipitate formation of this polymer. Another possible explanation for the precipita-

tion of the polymer is the formation of an aminal instead of an imine leading to crosslinking of the polymer. The polyfuroin, however, also contains other functional groups making other reactions possible as well.

4. Conclusions

We have shown that the polymerisation of 2,5-diformylfuran by NHC catalysts produces short oligomers that have a low thermal degradation temperature and no detectable crystallinity. The catalyst structure and duration of the polymerisation greatly influence the polymer molar mass. Reaction of the polymer with a multifunctional amine causes it to precipitate either by chain extension or crosslinking.

Author Contributions

Wouter Ruelens: methodology, formal analysis, investigation, data curation, writing – original draft, visualization Fariba Mafakheri: formal analysis, investigation, writing – review & editing Viktor Van Lierde: methodology, formal analysis, investigation, writing – review & editing Mario Smet: conceptualization, resources, writing review & editing, supervision, funding acquisition

Conflict of Interest

The author(s) declared no potential conflicts of interest with respect to the research, authorship, and/or publication of this article.

Funding

This research was funded by Research Foundation - Flanders, grant number G0D5416N.

Acknowledgments

The authors gratefully acknowledge Bart Van Huffel and prof. Wim De Borggraeve for their assistance and guidance on the DOSY measurements.

References

[1] Ogale, A.A., Zhang, M., Jin, J., 2016. Recent advances in carbon fibers derived from biobased precursors. Journal of Applied Polymer Science. 133, 45. DOI: https://doi.org/10.1002/app.43794

[2] Cai, C.M., Zhang, T.Y., Kumar, R., et al., 2014. Integrated furfural production as a renewable fuel and chemical platform from lignocellulosic biomass. Journal of Chemical Technology and Biotechnology. 89(1), 2-10. DOI: https://doi.org/10.1002/jctb.4168

[3] Huang, Y.B., Yang, Z., Dai, J.J., et al., 2012. Production of high quality fuels from lignocellulose-derived chemicals: a convenient C–C bond formation of furfural, 5-methylfurfural and aromatic aldehyde. RSC Advances. 2(30), 11211. DOI: https://doi.org/10.1039/c2ra22008c

[4] Hoydonckx, H.E., Van Rhijn, W.M., Van Rhijn, W., et al., 2007. Furfural and Derivatives. Ullmann's Encyclopedia of Industrial Chemistry. Wiley-VCH Verlag GmbH & Co. KGaA; Weinheim, Germany. DOI: https://doi.org/10.1002/14356007.a12_119.pub2

[5] Mariscal, R., Maireles-Torres, P., Ojeda, M., et al., 2016. Furfural: a renewable and versatile platform molecule for the synthesis of chemicals and fuels. Energy & Environmental Science. 9(4), 1144-1189. DOI: https://doi.org/10.1039/C5EE02666K

[6] Girka, Q., Estrine, B., Hoffmann, N., et al., 2016. Simple efficient one-pot synthesis of 5-hydroxymethylfurfural and 2,5-diformylfuran from carbohydrates. Reaction Chemistry & Engineering. 1(2), 176-182. DOI: https://doi.org/10.1039/C5RE00004A

[7] Sarmah, B., Srivastava, R., 2019. Selective two-step synthesis of 2,5-diformylfuran from monosaccharide, disaccharide, and polysaccharide using H-Beta and octahedral MnO_2 molecular sieves. Molecular Catalysis. 92-103. DOI: https://doi.org/10.1016/j.mcat.2018.11.001

[8] John, G., Nagarajan, S., Vemula, P.K., et al., 2019. Natural monomers: A mine for functional and sustainable materials – Occurrence, chemical modification and polymerization. Progress in Polymer Science. 92, 158-209. DOI: https://doi.org/10.1016/J.PROGPOLYMSCI.2019.02.008

[9] Fache, M., Darroman, E., Besse, V., et al., 2014. Vanillin, a promising biobased building-block for monomer synthesis. Green Chemistry. 16(4), 1987-1998. DOI: https://doi.org/10.1039/C3GC42613K

[10] Cao, L., Yu, I.K.M., Liu, Y., et al., 2018. Lignin valorization for the production of renewable chemicals: State-of-the-art review and future prospects. Bioresource Technology. 269, 465-475. DOI: https://doi.org/10.1016/j.biortech.2018.08.065

[11] Araújo, J.D.P., Grande, C.A., Rodrigues, A.E., 2010. Vanillin production from lignin oxidation in a batch reactor. Chemical Engineering Research and Design. 88(8), 1024-1032. DOI: https://doi.org/10.1016/j.cherd.2010.01.021

[12] Bello, S., Salim, I., Méndez-Trelles, P., et al., 2018. Environmental sustainability assessment of HMF and FDCA production from lignocellulosic biomass

through life cycle assessment (LCA). Holzforschung. 73(1), 105-115.
DOI: https://doi.org/10.1515/hf-2018-0100

[13] Motagamwala, A.H., Won, W., Sener, C., et al., 2018. Toward biomass-derived renewable plastics: Production of 2,5-furandicarboxylic acid from fructose. Science Advances. 4(1), eaap9722.
DOI: https://doi.org/10.1126/sciadv.aap9722

[14] Ma, J., Wang, M., Du, Z.,et al., 2012. Synthesis and properties of furan-based imine-linked porous organic frameworks. Polymer Chemistry. 3(9), 2346-2349.
DOI: https://doi.org/10.1039/c2py20367g

[15] Hui, Z., Gandini, A.,1992. Polymeric schiff bases bearing furan moieties. European Polymer Journal. 28(12), 1461-1469.
DOI: https://doi.org/10.1016/0014-3057(92)90135-O

[16] Wayne Cooke, A.B., Wagener, K., 2002. An investigation of polymerization via reductive coupling of carbonyls. Macromolecules. 24(6), 1404-1407.
DOI: https://doi.org/10.1021/ma00006a029

[17] Amarasekara, A.S., Green, D., Williams, L.D., 2009. Renewable resources based polymers: Synthesis and characterization of 2,5-diformylfuran–urea resin. European Polymer Journal. 45(2), 595-598.
DOI: https://doi.org/10.1016/j.eurpolymj.2008.11.012

[18] Pinaud, J., Vijayakrishna, K., Taton, D., et al., 2009. Step-Growth Polymerization of Terephthaldehyde Catalyzed by *N* -Heterocyclic Carbenes. Macromolecules. 42(14), 4932-4936.
DOI: https://doi.org/10.1021/ma900907f

[19] Liu, N., 2013. New polymers synthesis by organocatalyzed step-growth polymerization of aldehydic monomers : polyaldols, linear polybenzoin and hyperbranched polyacetals.
DOI: https://tel.archives-ouvertes.fr/tel-01081197

[20] Wöhler, L., 1832. Study on the radical of benzoic acid. Journal of Pharmacy (In German). 3(3), 249-282.
DOI: https://doi.org/10.1002/jlac.18320030302

[21] Ukai, T., Tanaka, R., Dokawa, T., 1943. A new catalyst for acyloin condensation. Journal of the Pharmaceutical Society of Japan. 63, 296-300.

[22] Flanigan, D.M., Romanov-Michailidis, F., White, N.A., et al., 2015. Organocatalytic Reactions Enabled by N-Heterocyclic Carbenes. Chemical Reviews. 115(17), 9307-9387.
DOI: https://doi.org/10.1021/acs.chemrev.5b00060

[23] Baragwanath, L., Rose, C.A., Zeitler, K., et al., 2009. Highly Enantioselective Benzoin Condensation Reactions Involving a Bifunctional Protic Pentafluorophenyl-Substituted Triazolium Precatalyst. The Journal of Organic Chemistry. 74(23), 9214-9217.
DOI: https://doi.org/10.1021/jo902018j

[24] Romanov-Michailidis, F., Besnard, C., Alexakis, A., 2012. N-Heterocyclic Carbene-Catalyzed Annulation of α-Cyano-1,4-diketones with Ynals, Organic Letters. 14(18), 4906-4909.
DOI: https://doi.org/10.1021/ol3022287

[25] Enders, D., Breuer, K., Kallfass, U., et al., 2003. Preparation and application of 1,3,4-triphenyl-4,5-dihydro-1H-1,2,4-triazol-5-ylidene, a stable carbene, Synthesis. 8, 1292-1295.
DOI: https://doi.org/10.1055/s-2003-39409

[26] Ma, Y., Wei, S., Wu, J., et al., 2008. From mono-triazolium salt to bis-triazolium salt: Improvement of the asymmetric intermolecular benzoin condensation. Advanced Synthesis and Catalysis. 350(16), 2645-2651.
DOI: https://doi.org/10.1002/adsc.200800371

[27] Smirnova, N.V., Klushin, V.A., Bezbozhnaya, T.V., et al., 2018. Selective Oxidation of 5-(Hydroxymethyl) furfural to Furan-2,5-dicarbaldehyde with Sodium Nitrite in Phosphoric Acid. Russian Journal of Organic Chemistry. 54(3), 414-418.
DOI: https://doi.org/10.1134/S1070428018030077

BILINGUAL PUBLISHING CO.
Pioneer of Global Academics Since 1984

Organic Polymer Material Research
https://ojs.bilpublishing.com/index.php/opmr

ARTICLE

Mechanical, Electrical and Thermal Properties of Nylon-66/Flyash Composites: Effect of Flyash

Shyam D Maurya[1*] Manoj K Singh[2] Syed Amanulla[2] S N Yadav[1] Sanjay K Nayak[3]

1. Central Institute of Petrochemicals Engineering & Technology, Lucknow, Uttar Pradesh, 226008, India
2. Central Institute of Petrochemicals Engineering & Technology, Hajipur, Bihar, 844101, India
3. Ravenshaw University, Cuttack, Odisha, 753003, India

ARTICLE INFO

Article history
Received: 04 November 2022
Revised: 07 December 2022
Accepted: 08 December 2022
Published Online: 30 December 2022

Keywords:
Nylon-66
Flyash
Composites
Voids
Morphology

ABSTRACT

In the current study, the effect of flyash (FA) on the physic-mechanical, electrical, thermal and morphological behavior of nylon-66 (PA) was investigated. PA/FA composites were prepared by melt mixing via twin screw extruder, with varying weight percent (5 wt %, 10 wt %, 15 wt % and 20 wt %) of flyash. The results of composites were optimized and compared with virgin nylon-66. Mechanical and electrical properties of composites improved up to 10 wt% of FA loading without compromising the properties. The flyash filled nylon-66 composites showed a low abrasive wear rate. Increase the heat distortion temperature of composites with an increase in weight percent of flyash while opposing the melt flow rate. Flyash filler enhances the stiffness of plastics but significantly reduces the impact properties. Dispersion of flyash was examined by impact fracture surface of composites using a scanning electron microscope.

1. Introduction

Presently around the world huge amount of industrial 'coal ash' waste is entity discharged from the thermal power plant. Many problems such as dumping sites and rising costs of its disposal have made it difficult to manage. For this motive, a range of methods to supportively use coal ash has been upward [1]. This a promising way to reuse flyash in the plastic industry, as plastic products are frequently compounded with flyash as an inorganic filler [2,3]. Flyash contains a variety of inorganic oxides and is available in powdered form, and this filler is mixed into plastic resins and alters the properties of composites. The properties of particulate-filled polymer composites depend sturdily on the shape, size and distribution of particulate filler in the polymer matrix. Flyash has been found to alter the composite hardness. Dielectric strength can improve by the larger polarization developed by material in an applied field of a given strength. Inorganic/ceramics

**Corresponding Author:*
Shyam D Maurya,
Central Institute of Petrochemicals Engineering & Technology, Lucknow, Uttar Pradesh, 226008, India;
Email: shyam4ucipet@gmail.com

DOI: https://doi.org/10.30564/opmr.v4i2.5233

materials usually have superior dielectric constant than polymeric materials [4]. Flyash contains more polar groups and ions, which contribute to its high dielectric properties. Also, these materials have higher thermal properties, and for this reason, the temperature must lead to an excessive end of the processing temperature. Bose et al. reported the effect of flyash on the thermal, mechanical, dielectric rheological and morphological properties of filled nylon 6. Flyash filled composite showed improved performance due to the interfacial interaction with polymer [3]. Similar results were also explained in Polyamide/flyash blends prepared via masterbatch preparation [5]. Liu L. et al. reported the inorganic filler with polyimide, and the results improve the dielectric constant. Flyash has been used in earlier studies individually as a filler in the polymer [6,7].

Engineering plastic such as nylon-66 are mostly used in the automobile sector, and electrical and home appliances, because of their excellent mechanical properties but few limitations. Many disadvantages of nylon-66 are they have low electrical and thermal properties. Hence various efforts have been undertaken to use for altering the properties of nylon-66 as a matrix for composite by adding flyash. This display shows a remarkable improvement in the dielectric and thermal properties of nylon-66/FA composites. Flyash composite properties can alter by varying the particle size of flyash [8-10], and variation in weight percent of flyash [11-13]. This study uses injection molding and has reported the mechanical thermal and electrical properties of flyash composites. Moreover, there has been little work done on estimating the melt flow rate, abrasive wear rate and electrical properties of flyash composite.

Hence, this studies nylon-66 with different weight percent of flyash composites prepared via melt mixing and evaluation. Physic-mechanical, melt flow rate, thermal and dielectric properties of nylon-66/flyash composites were investigated. Flyash offers a significant economic benefit more than competing fillers.

2. Experimental

2.1 Materials

Flyash was collected from Ennore Thermal Power Plant, Chennai India and nylon-66 was acquired from Tunfnyl-SRF, Ltd. Chennai India. The average diameter of flyash was less than 38 μm separated from flyash, with the help of a sieve sacker.

2.2 Melt Mixing and Pelletizing

Before mixing, the flyash and nylon-66 were dried at 120 °C and 80 °C respectively for 8 hours in a hot air oven. Different wt% (00, 05, 10, 15, and 20) of flyash mixed with nylon-66 and extrudate in a co-rotating twin screw extruder. The L/D ratio of the screw was 40:1. Extruder speed, 135-150 rpm was maintained for all compositions and extrudates were quenched in the tank at 20 °C ~ 30 °C and palletized. In all the above sets of experiments, 0.5 wt% of wax was mixed with antioxidants. The temperature profiles of the extrusion were zone 1 (230 °C), zone 2 (265 °C), zone 3 (280 °C), zone 4 (290 °C), zone 5 (285 °C), and die (275 °C). The rpm of the palletizer was maintained.

2.3 Sample Preparation

The materials were prepared in a hot air oven at 80 °C for 8 hours. Using the manual-based injection molding machine (M/s R. H. Windsor India Ltd.) fitted with mould containing cavity. After molding, ejections from the mould samples were packed in a dedicator. Moulding parameters were same for the all the formulations and temperatures set in zone 1 (260 °C), zone 2 (275 °C), and zone 1 (280 °C). Schematic presentations for mixing and sample preparation are shown in Figure 1.

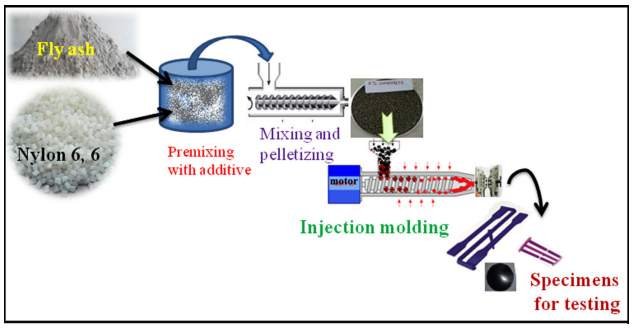

Figure 1. A schematic presentation of the procedure for mixing and specimen preparation

2.4 Characterization

2.4.1 Density and Void

Density measurements of nylon-66 and composite were evaluated as per ASTM D792-08 using single pan electronic weighing balance with the help of Equation (1):

$$\rho = \frac{w}{w - w_1} \times \rho_0 \quad (1)$$

where ρ 0 is the density of the liquid w is the weight of the sample in the air; w1 is the weight of the sample in the liquid. A minimum of five samples were measured and the average values of the density were accounted for. Theoretical densities (Td) of the composite were calculated with the help of Equation (2):

$$T_d = \frac{100}{\left(\frac{R}{D}\right) + \left(\frac{r}{d}\right)} \quad (2)$$

where, R = weight percent of the matrix in composite; D = density of matrix; r = weight percent of filler; and d = density of filler.

The void fractions of composites were calculated using Equation (3):

$$V = \frac{100(T_d - E_d)}{T_d} \quad (3)$$

where, V is the void content in the composites; T_d and E_d represent the theoretical and experimental densities of composites, respectively.

2.4.2 Mechanical Properties

The tensile strength of nylon-66 and its composite were calculated as per the ASTM D 638 test method using a Universal Testing Machine (Instron-3382 UK) with a crosshead scan speed of 10 mm/min. Dumbbell-shaped specimens with a dimension of (165 × 12.7 × 3) mm3 were subjected to the tensile strength measurement. An average of five samples were taken for each analysis and reported. The flexural strength and modulus of composites were analyzed as per the ASTM D790 method, using UTM (Instron-3382 UK). The specimens of the dimension (172 × 12.7 × 3) mm3 with the three-point bending mode at 100 mm span length and crosshead speed 2.0 mm/min.

The impact strength of the composite was determined according to ASTM D256 using an impact strength tester (Tinius Olsean, USA) and notch cutter. The specimen of dimension (65 × 12.7 × 3) mm3 and 2.54 deep standard V-notch was impressed on each sample. The unit of impact strength is J/m. The shore D hardness was determined as per ASTM D 2240 on the specimen with a thickness of 3 mm.

2.4.3 Abrasive Wear Rate

Abrasive wear analysis of nylon-66 and its composites were studied using an abrasion wear (M/s Taber Model 530 Abrader) testing machine. The test was conducted using the disc shape specimen of 100 mm diameter and 3 mm thickness. The sample was held against the rotating platform and gripped at a constant load of 4.9 N for 15 minutes and the sample weights before and after the tests are noted. Materials of higher wear resistance will have a lower volume loss. The test was conducted using a calibrated CS-10 wheel. The Taber wear index is evaluated using Equation (4) [14]:

$$\text{Wear index} = \frac{(\text{initial weight} - \text{final weight})}{\text{time of test cycle}} \times 1000 \quad (4)$$

where, the initial and final weights of samples are in grams, and the time of the test cycle is in minutes.

2.4.4 Electrical Properties

Dielectric strength was measured by CEAST-ITALY (ASTM D149). The configurations of the apparatus were 240 V, 50 Hz and 1 PH; output 0-60 kV; capacity 100 mA electrical instrument and using Equation (5):

$$\text{Dielectric strength} = \frac{\text{Breakdown voltage (v)}}{\text{Thickness (mm)}} \quad (5)$$

Measurement for the dielectric strength specimen is 100 mm diameter and 3 mm thickness and typically tested in oil to decrease the chance of flash over before break down. The dielectric constant of the composite was measured using Hewlet Packard 4284 1 20 Hz and 1 PH (ASTM D 150). Dimension for the dielectric strength specimen is 50 mm diameter and 3 mm thickness. Volume and Surface resistivity was measured by using Teraohmeter, (Ceast Italy) as per ASTM D 257-07. Specification for the measurement is 100 mm diameter with 3 mm thickness.

2.4.5 Heat Deflection Temperature (HDT)

The heat deflection temperature of nylon-66 and its composites were evaluated using an HDT analyzer (M/s GoTech, Taiwan), as per ASTM D648. The specimens of dimension (172 × 12.7 × 3) mm3 with a load of 0.15 MPa and heating rate of 2 °C/min.

2.4.6 Water Uptake Performance

The water absorption of nylon-66 and its composites was estimated as per ASTM D570. The specimen of dimension (76.2 × 25.4 × 3) mm3 was prepared and dried in a vacuum oven at 80 °C for 24 h, cooled in desiccators, and then instantly weighed. Subsequently, the weighed samples were deep in distilled water for 7 days at room temperature. The data reported are from an average of five samples. The percentage of water absorption was calculated using Equation (6):

$$\text{Water absorption (\%)} = \frac{(w_2 - w_1)}{w_1} * 100 \quad (6)$$

where w_1 is dried sample and w_2 is swollen sample.

2.4.7 Melt Flow Rate (MFR)

The melt flow rate (MFR) of nylon-66 and its composites were evaluated as per the ASTM D1238 method at 230 °C and a load of 2.16 kg. MFR unit is g/10 min.

2.4.8 Scanning Electron Microscopy (SEM)

The topography of impact fractured surface of nylon-66 and composites was investigated using a Carl Zeiss (EVO MA 15) (Carl Zeiss limited, Germany) SEM with high tension voltage of 20 kV. The specimen was conditioned for 1 h and sputter-coated with gold/palladium before imaging.

3. Results and Discussion

3.1 Density and Void Contents of Composites

The density and void content value of the composite are summarized in Table 1. A density value represents the major advantage of plastics/composites over other materials, specifically lightweight. The weight percent of flyash increased in the virgin matrix the density value increased due to the incorporation of the high density of flyash [15]. The void content of composite ranges from 0.502% to 1.973% and is higher when the weight percent of flyash is more (Table 1). A high void percent of composites is mighty to the formation of agglomeration at a higher ratio of flyash. This void content affects the properties of the composite such as mechanical, thermal and electrical properties. The high void content of composites' greater susceptibility to water penetrates and deteriorates the properties of polymers.

3.2 Tensile Properties

Mechanical properties of composites depend to a greater extent upon the uniform distribution of flyash in the matrix. Tensile strength, tensile modulus and percent elongation values are shown in Table 2. The tensile strength of the composite was initially rising up to 10 wt% of flyash and further decreased. This may be due to the uniform distribution of flyash in the matrix and grant a large interfacial area of content, resulting in better interfacial adhesion [16]. Further above 10 wt% of flyash, decrease the tensile strength, this might be due to the agglomeration of flyash [17].

However, the tensile modulus of composites was higher than virgin nylon-66. An increase in the weight percent of flyash increase in the tensile modulus of composite was shown in Table 2. Further 20 wt% of flyash loading increases the tensile modulus. This might be due to the inherent rigidity of composites. This attributes that the strength increases with an increase in the surface area of filled particles which contributes to the stress transfer mechanism [18]. Furthermore, the percent elongations of composites decrease with an increase in the concentration of flyash loading. This might be due to higher filler loading may have a deficient matrix existing for contributing to the elongation [3].

3.3 Flexural Properties

The flexural strength and flexural modulus of nylon-66 and its composites are shown in Table 2. The flexural strength of composites increased up to 10 wt% of flyash loading and further decreased. The PA/FA-2 shows the highest flexural strength 114 MPa in comparison to others. This result indicates the flyash is uniformly distributed inside the matrix which acting a strengthening of materials; thus stiffness and flexural strength are higher [19-21]. Further, 20 wt% of flyash composite shows low flexural strength due to agglomeration of flyash after a certain concentration. This may be due to lacking a matrix for encapsulating individual filler particles. This is discussed in the morphology section. Moreover, the flexural modulus increased constantly with an increase in weight percent of flyash loading. This was reduced by the addition of maximum loading (20 wt%) of flyash which might be the saturation level of filler.

Table 1. Density and void content of different composites

Sample code	Flyash (< 38 μm) (%)	Theoretical density (Td) (g/cc)	Experimental density (Ed) (g/cc)	Void content (%)	Water absorption (%)
PA	00	...	1.135	...	1.70
PA/FA-1	05	1.164	1.158	0.502	1.40
PA/FA-2	10	1.194	1.187	0.559	1.41
PA/FA-3	15	1.226	1.207	1.561	1.43
PA/FA-4	20	1.259	1.235	1.973	1.48

Table 2. Tensile, flexural and Impact strength of nylon-66 and its composites

Sample code	Tensile Properties			Flexural Properties		Impact Strength (j/m)
	Tensile Strength (MPa) (± 2%)	Tensile Modulus (MPa) (± 2%)	Elongation at break (%)	Flexural Strength (MPa) (± 2%)	Flexural Modulus (MPa) (± 2%)	
PA	78.32	4026.1	6.2	110.8	3023.7	72.2
PA/FA-1	79.5	4179.1	5.1	112.6	3244.7	68.2
PA/FA-2	79.4	4140.4	4.9	113.9	3281.8	67.2
PA/FA-3	71.5	3921.1	4.2	103.6	3522.1	62.1
PA/FA-4	70.4	4298.2	3.2	98.3	3550.2	54.1

3.4 Hardness

The hardness values of composites are shown in Table 3. Virgin PA shows a very low hardness value as compared with other composites. Hardness increases for every 5 wt% rise in flyash content. This improvement in the hardness of composites can be explained by the action of indentation force in the polymer matrix phase and the flyash will be pressed together, touching each other and offering resistance resulting in the improvement of their hardness (Figure 2).

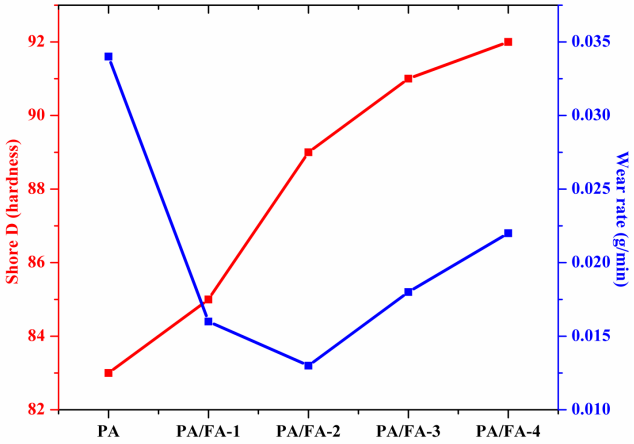

Figure 2. Effect of flyash on hardness and abrasive wear rate of composites

3.5 Impact Strength

The impact strength of composites with different weight percent of flyash are exposed in Table 2. The impact strength of composite decreased with an increase in wt% of filler. This was attributed to worse interface and dispersion at a higher weight percent of filler results decreased the stressed areas. This behavior shows an increased weight percent of filler decreased the capacity of the matrix to absorb energy consequently lowering the toughness. Thus, the elastic behavior of the matrix is directionally proportional to the filler loading.

3.6 Abrasive Wear Analysis

The abrasive wear rates of nylon-66 and its composites are exposed in Table 3. The abrasive wear rates of flyash filled composites are far less than the virgin nylon-66. Results show the presence of flyash reduces the abrasive wear rate of composites. It was observed that the abrasive wear rate of composites, sharply decreases with an increase in flyash content up to 10 wt%. Further the abrasive wear rate increases with the increase in flyash content but still it was less than the virgin nylon-66. This might be attributed to the combination of evidence such as the interfacial adhesion of the filler between matrixes [22]. This is associated with the increase in heat distortion temperature due to the filler content, and the ability of flyash to reduce the thermal softening of the polymer due to the interfacial heat developed during sliding. Results showed 10 wt% flyash-filled composites is better than other composition in perspective of wear.

Table 3. Heat distortion temperature, melt flow index and water absorption of composites

Sample code	HDT (°C)	MFI (gm/10 min)	Shore D Hardness	Abrasive wear (g/min)
PA	75	13.01	83	0.034
PA/FA-1	80	10.44	85	0.016
PA/FA-2	85	9.12	89	0.013
PA/FA-3	88	6.02	91	0.018
PA/FA-4	89	4.78	92	0.022

3.7 Electrical Properties

3.7.1 Dielectric Strength and Dielectric Constant

The dielectric strength and dielectric constant of composites are summarized in Table 4. The dielectric strength increased with the increase in flyash loading and was constant at higher wt%. This fashion in deviation of dielectric strength with filler is credited to the total surface area existing from the filler. This might be due to leakage of current from the unencapsulated flyash particle at higher loading [23]. The dielectric constant increased with an increase in flyash content, which might be due to the enlargement in the polarizability group with the inclusion of flyash which replaces a large part of the matrix [4]. Similar results were discussed with the increment of dielectric strength leakage of current from unencapsulated interstitial filler particles [3].

3.7.2 Surface and Volume Resistivity

Surface and volume resistivity show the ability of material resist against applied voltage. Increasing the flyash loading increase the volume and surface resistivity for optimum wt% further increase get the reduced value shown in Table 4. This shows the low wt% gives ultimate strength with 10 wt% composites. The lower the volume resistivity of a material is, the more conductive the material.

3.8 Thermal Properties

3.8.1 Heat Distortion Temperature

Improved heat distortion temperatures of composites by incorporating flyash are depicted in Table 3.

PA/FA-2 (10 wt%) filled flyash composites support

Table 4. Dielectric strength, dielectric constant, surface & volume resistivity of composites

Sample code	Dielectric strength(v/mm)	dielectric constant (10^{-6} Hz)	Surface Resistivity (Ohm)	Volume Resistivity (Ohm.m)
PA	5.23	2.91	$3.14*10^{14}$	$9.25*10^{13}$
PA/FA-1	7.4	3.22	$8.59*10^{14}$	$9.47*10^{13}$
PA/FA-2	8.5	3.28	$4.3*10^{14}$	$7.71*10^{14}$
PA/FA-3	8.6	3.31	$1.29*10^{14}$	$7.79*10^{14}$
PA/FA-4	8.6	3.42	$2.57*10^{14}$	$7.84*10^{14}$

13% higher heat distortion temperature. This shows high melting point flyash plays a significant role in sustaining the molecular chain in the matrix when the sample starts to soften. This improves in thermal stability and service temperature range of the composites. Further, HDT was higher at higher loading of flyash, which indicates higher filler loading.

3.8.2 Melt Flow Rate

The effect of flyash loading on the melt flow rate of PA/FA composites at standard conditions is summarized in Table 3. The melt flow rate decreases with increasing flyash loading (Figure 3) and so proper processing conditions are needed. This rate of decrease with volume fraction, may be due to the restriction of flow with flyash. Flyash has a high density in comparison to nylon-66 and poor interference between the flyash and matrix. Composites flow rate is invasively proportional to heat distortion temperature.

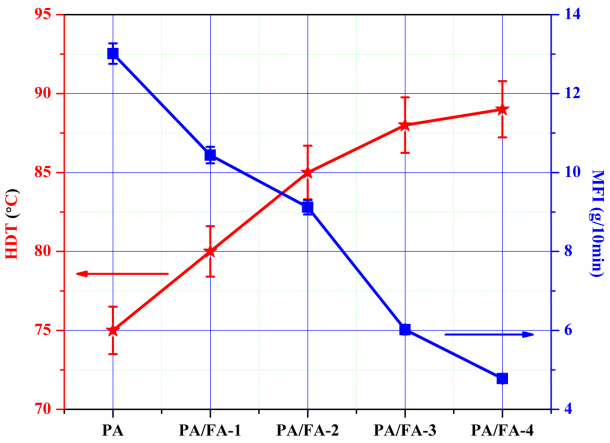

Figure 3. HDT and MFI of PA-66 composite effect of flyash loading on composites

3.9 Water Absorption Behavior

Water uptake capacities of the composite were found to decrease with the flyash weight percent increase exposed in Table 1 as a function of flyash loading. Nylon-66 is hygroscopic material due to polar groups in the backbone and easily penetrates water molecules in the virgin matrix. It is clearly marked that the nylon-66/flyash composites have low water absorption as compared to the virgin matrix due to the decreased polar group concentration which might affect the water absorption capacity in composites. PA/FA-4 shows more water uptake percent as compared with PA/FA-1. This may be due to the poor dispersion of flyash resulting increase pores which leads to low water absorption and the evidence shows in morphological behavior in the next section [19].

3.10 Fracture Surface Morphology of Composites

The fracture surface morphology of nylon-66 and its composites containing 5 wt%, 10 wt% and 20 wt% of flyash are shown in Figure 4 using SEM analysis.

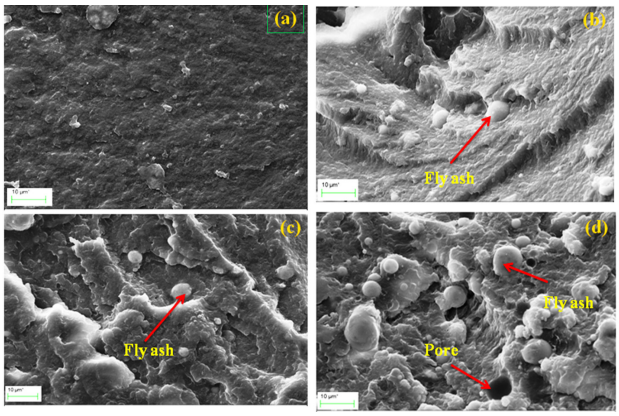

Figure 4. Impact fracture surface of (a) virgin PA-66 (b) 5% flyash (c) 10% flyash (d) 20% flyash with composite

It was observed that the fracture surfaces were rough and more ductile than nylon-66. The fracture surface of the composites shows filler is uniformly dispersed and matrixes pull out on the surface up to 10 wt% (Figure 4b and 4c). Very less debonded particles were observed which involves better interaction between the matrix with the filler at 10 wt% loadings and indicates enhanced polymer-filler adhesion. Further, 20 wt% of flyash particles form clusters (agglomerates), due to poor dispersion and pore-formed results easily debond (Figure 4d). Therefore low energy required for debonding of filler from the ma-

trix, leads to plausibly low impact strength. Similar results were observed that the matrix was insufficient to encapsulate the individual flyash particles investigate by morphology study [3].

4. Conclusions

The different weight percent of nylon-66/flyash composites were prepared by the melt mixing method. The higher loading of flyash notably decreased the tensile strength and flexural strength whereas modulus increased. The incorporation of flyash into nylon-66 shows higher dielectric properties. The impact strength of composites decreased whereas the hardness was increased up to 10 wt% compared to virgin polymer. Abrasive wear analysis shows that flyash reduces the material deletion rate of composites. Owing to the improved polymer filler interaction established by the water uptake behavior. However, the water tendency was higher at a higher wt% of flyash. This was attributed to the poor physical interface between the filler and the matrix due to clusters formed. Increase heat distortion temperature of composites with an increase in weight percent of flyash whereas opposing the melt flow rate. Fracture surface morphology shows the interaction between matrix with the filler at this loading. Overall results found that flyash acts as reinforcement in the polymer matrix.

Acknowledgments

The authors would like to thank Ennore thermal power plant for providing the flyash and Tunfnyl-SRF, Ltd. to supply Nylon-66.

Conflict of Interest

There is no conflict of interest.

References

[1] Ding, J., Ma, S., Shen, S., et al., 2017. Research and industrialization progress of recovering alumina from flyash: A concise review. Waste Management. 60, 375-387.

[2] Chris-Okafor, P.U., Onwuka, C.O., Anekwe, O.J., et al., 2021. Impact of mixed fillers on the physico-mechanical properties of flexible polyether foam. Organic Polymer Material Research. 3(1).

[3] Bose, S., Mahanwar, P.A., 2004. Effect of flyash on the mechanical, thermal, dielectric, rheological and morphological properties of filled nylon 6. Journal of Minerals and Materials Characterization and Engineering. 3(02), 65.

[4] Ahmad, Z., 2012. Polymer dielectric materials. Dielectric Material.
DOI: https://doi.org/10.5772/50638.

[5] Ez-Zahraoui, S., Kassab, Z., Ablouh, E.H., et al., 2021. Effect of fly ash and coupling agent on the structural, morphological, thermal, and mechanical properties of polyamide 6/acrylonitrile-butadiene-styrene blend. Polymer Composites. 42(7), 3518-3538.

[6] Liu, L., Liang, B., Wang, W., et al., 2006. Preparation of polyimide/inorganic nanoparticle hybrid films by sol-gel method. Journal of Composite Materials. 40(23), 2175-2183.

[7] Venkatachalam, G., Kumaravel, A., 2017. Mechanical behaviour of aluminium alloy reinforced with sic/flyash/basalt composite for brake rotor. Polymers & Polymer Composites. 25(3), 203-208.

[8] Devi, M.S., Murugesan, V., Rengaraj, K., et al., 1998. Utilization of flyash as filler for unsaturated polyester resin. Journal of Applied Polymer Science. 69(7), 1385-1391.

[9] Bonda, S., Mohanty, S., Nayak, S.K., 2012. Viscoelastic, mechanical, and thermal characterization of flyash-filled ABS composites and comparison of flyash surface treatments. Polymer Composites. 33(1), 22-34.

[10] Cai, Z., Wang, X., Luo, B., et al., 2017. Dielectric response and breakdown behavior of polymer-ceramic nanocomposites: The effect of nanoparticle distribution. Composites Science and Technology. 145, 105-113.

[11] Setsuda, R., Fukumoto, I., Kanda, Y., 2012. Effects of flyash in composites fabricated by injection molding. Polymer Composites. 33(8), 1351-1359.

[12] Zhang, J., Du, Z., Zou, W., et al., 2017. MgO nanoparticles-decorated carbon fibers hybrid for improving thermal conductive and electrical insulating properties of Nylon 6 composite. Composites Science and Technology. 148(18), 1-8.
DOI: https://doi.org/10.1016/j.compscitech.2017.05.008.

[13] Ahmad, I., Mahanwar, P.A., 2010. Mechanical properties of flyash filled high density polyethylene. Journal of Minerals and Materials Characterization and Engineering. 9(03), 183.

[14] American Society for Testing and Materials (ASTM) [Internet], 1997. Annual Book of ASTM Standards, Philadelphia, USA. Available from: https://www.astm.org/products-services/bos.html.

[15] Alaneme, K.K., Sanusi, K.O., 2015. Microstructural characteristics, mechanical and wear behaviour of aluminium matrix hybrid composites reinforced with alumina, rice husk ash and graphite. Engineering Science and Technology, an International Journal.

18(3), 416-422.

[16] Rama, S.R., Rai, S.K., 2010. Studies on physicomechanical properties of flyash-filled hydroxyl-terminated polyurethane-toughened epoxy composites. Journal of Reinforced Plastics and Composites. 29(14), 2099-2104.

[17] Chaowasakoo, T., Sombatsompop, N., 2007. Mechanical and morphological properties of flyash/epoxy composites using conventional thermal and microwave curing methods. Composites Science and Technology. 67(11), 2282-2291.

[18] Ramesan, M.T., 2014. Effect of flyash on thermal stability, flammability, oil resistance and transport properties of chlorinated styrene butadiene rubber composites. Journal of Elastomers & Plastics. 46(4), 303-324.

[19] Fu, S.Y., Feng, X.Q., Lauke, B., et al., 2008. Effects of particle size, particle/matrix interface adhesion and particle loading on mechanical properties of particulate–polymer composites. Composites Part B: Engineering. 39(6), 933-961.

[20] Ramakrishna, H.V., Priya, S.P., Rai, S.K., 2006. Effect of flyash content on impact, compression, and water absorption properties of epoxy toughened with epoxy phenol cashew nut shell liquid-flyash composites. Journal of Reinforced Plastics and Composites. 25(5), 455-462.

[21] Sreekanth, M.S., Joseph, S., Mhaske, S.T., et al., 2011. Effects of mica and flyash concentration on the properties of polyester thermoplastic elastomer composites. Journal of Thermoplastic Composite Materials. 24(3), 317-331.

[22] Kilinçarslan, Ş., Türker, Y.Ş., 2020. Investigation of wooden beam behaviors reinforced with fiber reinforced polymers. Organic Polymer Material Research. 2(1).

[23] Setsuda, R., Fukumoto, I., Kanda, Y., 2012. Effects of flyash in composites fabricated by injection molding. Polymer Composites. 33(8), 1351-1359.

BILINGUAL PUBLISHING CO.
Pioneer of Global Academics Since 1984

Organic Polymer Material Research
https://ojs.bilpublishing.com/index.php/opmr

ARTICLE

Understanding the Effect of Zinc Oxide (ZnO) With Carbon Black Coupling Agent on Physico-Mechanical Properties in Natural Rubber Matrix

Koushik Pal* **Koushik Banerjee** **Soumya Ghosh Chowdhury** **Sanjay Kumar Bhattacharyya** **Rabindra Mukhopadhyay**

Hari Shankar Singhania Elastomer and Tyre research Institute, Plot No. 437, Hebbal Industrial Area, Mysore, Karnataka, 570016, India

ARTICLE INFO

Article history
Received: 23 December 2022
Revised: 20 February 2023
Accepted: 21 February 2023
Published Online: 01 March 2023

Keywords:
Carbon black
Natural rubber
Carbon black coupling agent
Anti-reversion properties

ABSTRACT

Natural rubber (NR) is not only the main compounding ingredient used to make the majority of components of tires as well as other rubber products, as it plays a significant role in ensuring that they operate well and complies with environmental standards. The applications of NR products are limited to high temperatures due to the revision tendency of NR vulcanizate. To address these issues, the potential engagement of a carbon black (CB) coupling agent (CA) in the presence of metal oxide i.e. Zinc Oxide (ZnO) was investigated in an NR-based system. This CA has dual functionality on physicomechanical properties. CA has the ability to reduce hysteresis loss as well as improve anti-reversion properties and these properties thoroughly depend on the presence of ZnO. While ZnO was added to the master formulation, a 65% improvement in reversion properties was observed. On the other hand, while ZnO fully transferred to the final formulation, bound rubber (BR) content increased by 19%, the difference in storage modulus (ΔG') is reduced by 22%, cure rate index (CRI) improved by 14%, loss tangent (tan δ) reduced by 18% and slightly improve in elongation at break compared to control compound. Thermo-gravimetric analysis (TGA) was engaged to understand the thermal stability and degree of purity of CA. A differential Scanning Calorimeter (DSC) was used to detect the phase transition of CA. Fourier Transform Infrared Spectrum (FTIR) was adopted to detect the presence of carboxyl and amine groups in the CA moiety. Payne effect, BR content and Transmission Electron Microscope (TEM) were employed to investigate the micro-level dispersion of CB in the natural rubber (NR) matrix.

**Corresponding Author:*
Koushik Pal,
Hari Shankar Singhania Elastomer and Tyre research Institute, Plot No. 437, Hebbal Industrial Area, Mysore, Karnataka, 570016, India;
Email: koushik.pal@jkmail.com; pst.koushik@gmail.com

DOI: https://doi.org/10.30564/opmr.v4i2.5341

1. Introduction

There has been a huge demand to improve the fuel efficiency in passenger car tires as well as truck tires because of the increasing fuel price, greenhouse gas emission and implementation of government regulations on rolling resistance (RR) [1-6]. RR loss of a tire can be defined as the mechanical energy consumed when the tires roll over on the road surface for a unit distance [7,8]. RR is directly related to the loss tangent (tan δ) of the compound. RR greatly enhances overall energy loss and has a direct impact on the fuel efficiency of a motor vehicle. As the rubbers are bad conductors of heat, there is an energy loss which leads to increased tire temperature during the running condition. The increase in temperature is effective on the reinforcement of the tire and ultimately its impact falls on the results as tread cuts and chips, treadwear and durability of the tire [4,9]. RR, mileage and durability are the three most considerable parameters for tire performance. So, there is a big challenge for researchers in this field to improve RR without compromising other properties.

A proper approach to the selection of rubber, chemicals and filler can significantly improve the tire properties [10]. Green compound properties can be improved through good dispersion of filler into the polymer matrix during mixing [11]. On the other hand, prolonged degradation of cured rubber can be achieved by using suitable anti-degradants. Generally, high structure and high surface area carbon blacks (CBs) are used in tire tread compound formulation to achieve better durability [12]. CB materials are aggregates of nanoparticles of spheroidal shape, typically 10-100 nm in diameter. The shape and degree of inter-linking of the aggregates are known as structure [13]. A "high structure" is characterized by extensive interlinking or branching, whereas a "low structure" is characterized by less pronounced interlinking or branching. In this experimental study, we used N134 CB, which has a particle size in the range of 11-19 nm. For this reason, the particles have a high tendency to form large aggregates of three-dimensional structure owing to their high surface area (the average surface area of N134 is 120-150 m^2/gm). This high tendency to form large aggregates makes N134 CB into high-structure CB. It is difficult to mix this type of CB with rubber because of high shearing and heat generation during mixing. To overcome this, plasticizers and oils are included in the compound formulation. CBs and silica are the two most widely used fillers for tire tread formulation. It is well known that incorporation of silica in rubber matrix is very difficult because of its reverse polarity in comparison with most of the rubbers (rubber is hydrophobic in nature and silica is hydrophilic) [14,15]. To address this, various silane coupling agents are used to create a bridging medium between rubber and silica. Similarly, to disperse CB into rubber moiety, using CB coupling agents (CA) came into the picture. Soumya et al. already discussed the potential of Sumilink 200, used as a CB CA for natural rubber tread compound formulation [16]. González et al. studied the influence of CB CA to improve the wet grip and RR of tires [17].

Heat generation in tire components also influences the aging rate of cured rubber compounds, and the effect of heat aging results in the polymer chain bond breakdown (softening) or conversion of Polysulfidic linkage to mono or di-sulfidic linkage (hardening), which mainly depends on the type of rubber and rubber chemicals used in rubber compound formulation [18,19]. This degradation of the rubber compound leads to a shorter service life of the tire. To achieve prolonged aging of the rubber compound, it is necessary to use the proper anti-aging chemical in the compound formulation.

In this study N'-methylidene-3-hydroxynaphthalene-2-carbohydrazide is used as a novel CA to improve CB dispersion. Its chemical structure is shown in Figure 1. Amine ($-NH_2$) and hydroxyl (-OH) are the two different functional groups present in this chemical. The reactivity and functionality of this chemical enhances based on the presence of ZnO. In the absence of ZnO, CA fully functioned as a CB CA, while in the presence of ZnO it acts as a CB CA as well anti-reversion agent. There are few articles available, where researchers studied the influence of CB CA agents on rubber properties [18,20,21]. But, other than coupling efficiency, other properties evaluations for this type of chemical have been not yet done before. Our present study is carried out on an NR-CB-based system having CA and ZnO in the compounding formulation. In this study we are trying to investigate the reactivity on coupling efficiency of CA in absence of ZnO. On the other hand, we have split out ZnO dosage in the master and final recipe. The intention of this study is to find out the suitable dosage of ZnO and CA for obtaining the least heat generation as well as reversion.

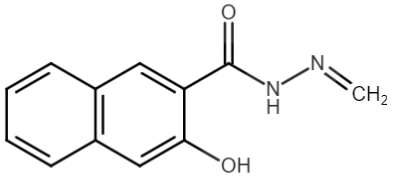

Figure 1. Molecular structure of N'-methylidene-3-hydroxynaphthalene-2-carbohydrazide.

2. Materials and Methods

2.1 Raw Materials

Natural rubber with grade SMR-20 (NR) was procured from Rubber Net (Asia) PTE Ltd., Indonesia and CA was supplied by Otsuka Chemical Private Ltd. (India). The other ingredients were used for this study as follows: N134 CB (Hi-tech Carbon Black Ltd, India), Zinc Oxide (ZnO) was supplied by POCL enterprises Ltd, Puducherry, India. The particle size of ZnO is in the range of 200 nm to 300 nm having an average particle size in the range of 250 nm. Stearic acid (VVF Ltd., India), Soluble sulfur (The Standard Chemical Co. Pvt Ltd.) and n-Cyclohexylbenzothiazol-2-sulphenamide (CBS) (Shandong Derek New Materials Co Ltd., Shandong, China).

2.2 Thermal Analysis

Thermo Gravimetric Analysis (TGA) of CA was performed by using Pyris-1 TG analyzer of Perkin-Elmer (Shelton, CT, USA) to understand the thermal degradation behavior of CA. This chemical was tested at a heating rate of 10 °C/min. The analysis was done by increasing the temperature from room temperature to 590 °C under a nitrogen atmosphere. During testing, the nitrogen atmosphere was used to create an inert atmosphere by preventing oxidative degradation.

To understand the reactivity of CA, Differential Scanning Calorimeter (DSC) with DSC 25 system (TA Instruments, Discovery series) was used. The analysis was done at a heating rate of 10 °C/min.

2.3 FTIR Study

Fourier Transform Infrared Spectroscopy (FTIR) of Perkin Elmer (Norwalk, CT, USA) was used to carry out micro-structure analysis of CA. The scanning range was from 500 cm^{-1} to 4000 cm^{-1} at a resolution of 4 cm^{-1} to record the spectrum.

2.4 Preparation of Rubber Compound

All the compounds were mixed as per the formulation and corresponding mixing sequence mentioned in Table 1 and Table 2 respectively. The reaction between CA, NR and CB generally happened between 145-150 °C. So, during master batch mixing, we maintained this specific range of temperature for two minutes. The mixing for all the stages i.e. masters, repass and final was conducted in lab scale Banbury mixer (Stewart Boilling, USA). This Banbury was equipped with a two-wing rotor with a 1.6 L capacity. The temperature control unit (TCU) was maintained at 90 °C for master and repass and 70 °C for final mixing.

Table 1. Detail formulation of the compounds.

Master					
Ingredients	Control	Exp 1	Exp 2	Exp 3	Exp 4
SMR20	100				
N134 Carbon Black	44				
Zinc Oxide	5	1	1.5	2.5	0
Stearic Acid	2				
CA	0	0.8			
Final					
Ingredients	Control	Exp 1	Exp 2	Exp 3	Exp 4
Zinc Oxide	0	4	3.5	2.5	5
Standard Sulphur	1.1				
CBS	1.7				

Table 2. Mixing sequence followed during Master, Repass and Final stage.

Time (sec)	**Actions taken**
MASTER Mixing Sequence	
0	Loading of the raw rubber and masticated for 30 sec at 50 rpm
30	Ram up and added carbon black and other chemical, ram down at 50 rpm
120	Ram sweep and ram down at 50 rpm
180	Ram sweep and ram down at 50 rpm
180-300	Maintain temperature at 145-150 °C
300	Ram up and discharge the batch
REPASS Mixing Sequence	
0	Load the master batch and ram down at 50 rpm
90	Ram sweep and ram down at 50 rpm
180	Ram up and batch discharge at 150 °C
FINAL Mixing Sequence	
0	Load the repass batch along with final chemicals and ram down at 30 rpm
90	Ram sweep and ram down at 30 rpm
180	Ram up and batch discharge

2.5 Cure Characteristics

The cure characteristic of the final compounds was measured by using P-MDR (model RPA 2000, Alpha technologies, Akron, OHIO, USA). From the rheometric curve minimum torque (M_L), maximum torque (M_H), scorch time (ts_2) and optimum cure time (t_{90}) were generated. Where ts_2 corresponds to the time to rise 2-unit torque above the M_L value and tc_{90} is the time required to achieve 90% of the M_H value. tc_{90} of the compounds was deter-

mined by using Equation (1):

$$\text{Torque at 90\% cure} = 0.9\,(M_H\text{-}M_L) + M_L \quad (1)$$

The cure rate index (CRI) stands for the rate of curing and was determined by the following Equation (2).

$$CRI = \frac{100}{(tc_{90} - ts_2)} min^{-1} \quad (2)$$

The reversion of the compounds was calculated by using the following Equation (3).

$$Reversion\ \% = \frac{Max\ Torque - Final\ Torque}{Max\ Torque} \times 100 \quad (3)$$

2.6 Payne Effect

Dispersion of filler into rubber matrix was determined by Payne effect study. Shear storage modulus (G') at 1% to 100% strain at 50 °C and 1.67 Hz was measured by using Rubber Process analyzer (model RPA 2000, Alpha technologies, OHIO, USA). The difference in shear modulus at 0.1% and 100% (ΔG') is known as Payne effect of the compound. ΔG' values were calculated based on the following Equation (4).

$$\Delta G' = G'at\ 0.1\%\ strain - G'at\ 100\%\ strain \quad (4)$$

2.7 Bound Rubber Content

The solvent extraction process was used to determine the bound rubber (BR) content of the final compounds. 0.2-0.3 gm of rubber samples were duly packed inside a dried filter paper and keep it overnight in toluene solvent at 115-120 °C for extraction by using the Soxhlet apparatus. After complete extraction, the samples were kept in a hot air oven at 80 for one-two hours until they reached a constant weight. The total BRC percentage of the rubber compounds was calculated by using the following Equation (5) [22,23].

$$Total\ BRC\ (\%) = \frac{W_f - W(\frac{m_f}{m_f + m_p})}{W(\frac{m_p}{m_f - m_p})} \quad (5)$$

where W_f, W, m_f and m_p were denoted as final weight, initial weight, filler loading (%) and polymer loading (%) respectively.

2.8 Moulding

To prepare tensile slabs from the final compounds, moulding was performed (ASTM D3182) in an electrically heated hydraulic press (Hind hydraulics, India). The samples were cured at 145 °C for $2tc_{90}$ under 15 MPa pressure. To test the abrasion resistance of the compounds in the laboratory abrasion tester (LAT 100), samples were cured in a specially designed mould at 141 °C for 60 min under 15 MPa pressure. The dimension of the tensile slab and LAT 100 samples were 0.15 m/0.15 m/0.002 m (length/width/thickness) and 0.08 m/0.035 m/0.18m (outer diameter/width/thickness) respectively.

2.9 Tensile Properties

Tensile properties from the cured slabs were measured according to ASTM D412 by using a universal testing machine (UTM, Z010, Zwick/Roell, Germany). The testing was conducted at a speed of 500 mm/min at room temperature. The various tensile properties like moduli at different percent elongation, tensile strength (TS) and elongation at break (EB) were generated from the tensile curve [24,25]. The hardness of the cured slabs was measured by a multi-unit hardness tester (MUHT) as per ASTM D2240.

2.10 Dynamic Mechanical Analysis (DMA)

Storage modulus, loss modulus and loss tangent (tan δ) were measured by using a Dynamic mechanical analyzer (Model VA4000, manufactured by Metravib, France). Samples were prepared from cured slabs having a dimension of 10 mm/24 mm/2 mm (width/length/thickness) with a testing area of 10 mm. Samples were run at three specific temperatures (30 °C, 70 °C and 100 °C) at 5% strain with a frequency of 11 Hz.

2.11 TEM Images

Micro-level filler dispersion of reinforcing filler was captured by using high-resolution transmission electron microscopy (HRTEM), 200 kv Talos- S (FEI, Hillsboro, OR, USA). The samples were prepared by Ultra-microtomy (Leica Ultracut UCT) at –100 °C with a thickness of around 100 nm.

2.12 LAT 100 Testing

The abrasion resistance of the compounds was measured according to ISO/DIN 23233 by using Laboratory Abrasion Tester 100 (LAT 100, m/s VMI, Holland). The details testing configuration of this study are mentioned in the 3.9 LAT100 results section. The loss in mass of the test sample was measured and the loss per unit running distance was calculated as per Equation (6).

$$A = \frac{m}{s} \quad (6)$$

where, *A* is the loss in mass per unit running distance during the run, in mg/km; *m* is the loss in mass during the run, in mg; and *s* is the running distance, in km.

The wear rating was determined by comparing the loss in mass of the test sample per unit running distance with the loss in mass per unit running distance of the control

compound tested under the same condition. The rating of the tested compounds was assigned based on low, medium and high severity conditions as per the load speed and slip angles maintained during the testing. Based on the severity conditions, the average wear rating was estimated for the compounds.

3. Results and Discussion

3.1 Material Characterization

Thermogravimetry (TG) and differential thermogravimetry (DTG) profile is presented in Figure 2(A). The curve shows a two-step degradation. Degradation at 331 °C and 630 °C indicate the molecular breakdown of CA. No volatile loss was observed within the temperature range of 90-180 °C. The characteristic peaks present in CA indicate the material is pure and free from other contaminants. From the TGA curve, it is clear that CA is thermally stable up to 331 °C and therefore can be mixed with rubber without thermal degradation.

DSC is a useful tool to get thermal safety-related information such as the heat of reaction (ΔH), exothermic onset temperature (T_o) and a peak of temperature (T_p) [26]. Figure 2(B) depicts the calorimetric curve of CA. This clearly defines the fact that at around 150 °C, CA undergoes an intra molecular reaction. This may also be explained in a way that the activation energy corresponds to 150 °C, activates CA to become reactive. Thus, the improvement of any composite containing CA only shows improvement after mixing which is around 150 °C.

The FTIR spectrum of CA is shown in Figure 2(C). Definite transmittance at 3409 cm^{-1} is clearly evident in the presence of primary and secondary amine groups, whereas absorbance maxima at 1642 cm^{-1} attributed to "-C═O" stretching of amide group presence in CA moiety [27]. The presence of such amide and carboxyl functional groups in CA is likely to create an environment for the interaction with the surface polar groups of CBs.

3.2 Cure Characteristics

The effect of ZnO and CA on cure characteristics of NR-CB based compounds at 145 °C for 60 min is shown in Table 3. From the test results, it is observed that M_H value is the least and reversion percent is higher for Exp 4 compound compared to other variants. While the amount of ZnO (in phr) is gradually increased in a master batch of Exp 1, Exp 2 and Exp 3 compound formulation and it is observed that M_H value is much higher compared to Exp 4 compound. On the other hand, reversion percent also gradually decreases and it is the least for Exp 3 compound. This change can be explained based on the reaction mechanism, which is discussed in section 3.4. Due to the formation of a stable six-member ring between ZnO, hydroxyl group and amine group are present in CA, which improves the solubility and reactivity of ZnO. As a result, the formation of shorter sulfur crosslinks increases, which reflects in higher M_H value and lowering reversion percent against Exp 4 compound.

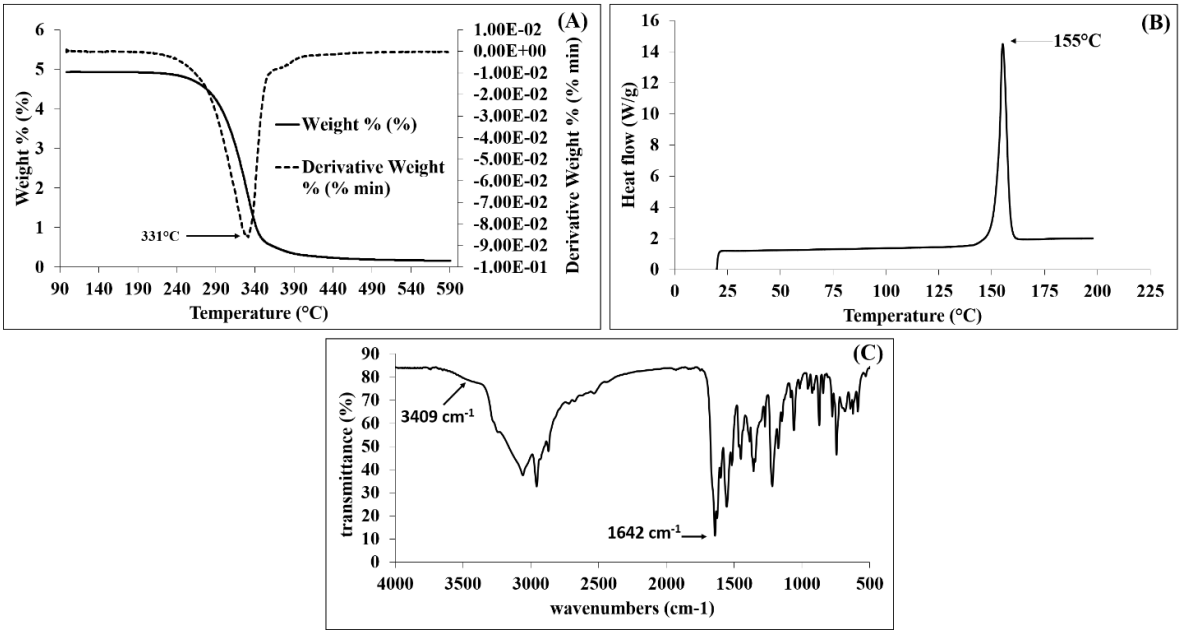

Figure 2. (A) TGA Curve, (B) DSC Curve, (C) FTIR Spectrum of CA.

Another interesting point that needs to be looked into is that the cure rate index (CRI) of Exp 4 compound is higher than others. This may be due to the presence of a higher amount of unreacted ZnO in the final batch for Exp 4 compound. A larger number of ZnO can react with the accelerator to generate an active Zn-accelerator complex which then accelerate the vulcanization reaction.

Table 3. Rheometric properties of all the formulations at 145 °C/60 min.

Rheometric Properties	Control	Exp 1	Exp 2	Exp 3	Exp 4
M_L (dNm)	2.98	3.54	3.59	3.42	3.38
M_H (dNm)	18.89	19.75	19.53	19.29	16.72
M_H-M_L (dNm)	15.91	16.22	15.93	15.87	13.35
ts_2 (min)	10.37	9.41	9.58	9.69	9.63
tc_{40} (min)	12.10	10.60	10.77	10.82	10.60
tc_{90} (min)	17.07	16.35	16.88	16.79	15.51
final torque (dNm)	18.49	19.56	19.35	19.14	16.36
% Reversion	2.15	0.97	0.93	0.76	2.16
CRI	14.93	14.41	13.70	14.08	17.01

3.3 Reaction Mechanism

As we have already mentioned that CA has a dual-functioning ability; it acts as a coupling agent as well as an anti-reversion agent. The coupling activity is plausible because of the presence of two reactive sites in the CA moiety, hydrazide group and pi-electron cloud of the naphthalene group. During mixing, due to shear force, active radicals are formed in NR chains which then react with the hydrazide group of CA. On the other hand, pi-electron of naphthalene group physically reacts with functional groups present in the CB. In this way, CA shows the coupling reactivity with NR and CB. The reaction mechanism is presented in Figure 3(A).

CA is also functioning as an anti-reversion agent due to the presence of ZnO in the reaction medium. The hydroxyl groups and amine groups present in CA form a stable six-member ring with ZnO, which results in increasing the solubility and reactivity in the rubber matrix. Higher ZnO reactivity results in the formation of shorter sulfur crosslinks, which improves compounds' thermal properties also. After the formation of this ZnO complex, CA has less opportunity to react with NR for the NR-CB coupling effect. A details reaction mechanism is shown in Figure 3(B).

3.4 Bound Rubber (BR)

BR gives an idea about the rubber-filler interaction in the uncured state. Physical and chemical interactions are supposed to involve during BR formation. In this matter of CB dispersion, free radical interaction between the filler surface groups and the polymer is proposed as a mechanism for BR formation [16]. The BR content of the uncured compounds is shown in Figure 4. It is observed that BR content is higher for Exp 4 compound. This result suggests that the interaction between rubber-filler improves in absence of ZnO. It is also observed that there is a gradual decrement of BR content value from Exp 1 to Exp 3 compound. This is because of the gradually increased ZnO phr in the formulation. Presence of ZnO leads to a lowering affinity of CA on CB dispersion. These trends of results are strongly supported by the Payne effect values, which are discussed in section 3.5.

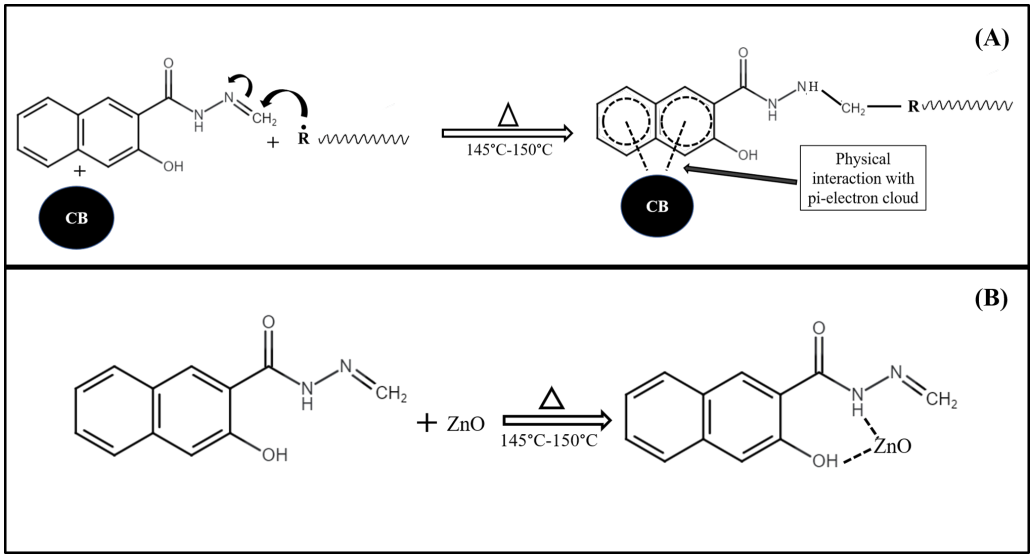

Figure 3. (A) and (B) reaction mechanism between Natural rubber, CA and ZnO.

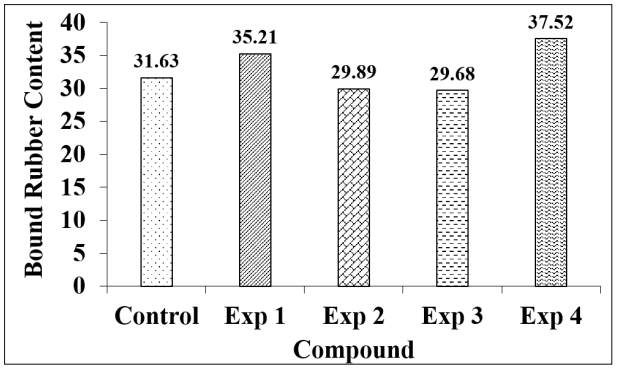

Figure 4. Bound rubber of the compounds.

3.5 Payne Effect

Payne effect of the green compounds is shown in Figures 5(A) and 5(B). From the results it is clear that inclusion of ZnO in final formulation reduces the Payne effect as compared to ZnO added in the master formulation. The gradual increase in Payne effect value from Exp 1 to Exp 3 confirms the less dispersion of filler in the polymer matrix. For Exp 4 compound, a lower ΔG' value implies better CB dispersion compare to control compound.

3.6 Physical Properties

Mechanical properties of the control and the experimental compounds are shown in Table 4. It was observed that there was a marginal drop in high strain modulus (M200, M300) in the experimental compounds. The TS and EB remained unaltered. In fact, there was a decent improvement found in elongation properties of the experimental compounds. Exp 4 showed the best combination of properties among the variants tested. From the results, it was evident that the addition of CA did not deteriorate the mechanical properties of the compounds; rather it improved the EB and toughness. The combination of tensile strength and EB leads to materials of high toughness [28,29]. EB and toughness are the two fundamental reinforcing properties of a rubber compound. When ZnO was used completely in the final batch (i.e. Exp 4), it was able to react chemically with CA in a more effective way such that the best properties were obtained in the compound. Exp 4 compound exhibit a higher toughness value, which actually indicates better dispersion of filler. This improvement in filler dispersion strongly correlates with BR and Payne effect values, which are discussed in section 3.4 and section 3.5 respectively. However, it has to be observed under dynamic conditions how CA would affect the compound properties.

Table 4. Physical properties at 145 °C/2tc_{90}.

Physicals Properties	Control	Exp 1	Exp 2	Exp 3	Exp 4
M100 (MPa)	2.3	2.2	2.3	2.3	2.2
M200 (MPa)	6.7	6.0	6.3	6.2	6.3
M300 (MPa)	13.6	12.4	12.7	12.5	13.0
Tensile Strength (MPa)	29.6	29.4	29.2	29	30.2
Elongation at Break (%)	513	537	530	522	530
Hardness (Shore A)	60	61	61	61	59
Toughness (J/m^3)	15185	15788	15476	15138	16006

3.7 DMA Results

The visco-elastic properties of the rubber compounds are mentioned in Table 5. It has been noticed that tan δ decreases progressively with a comparable dynamic stiffness value (E') while total ZnO is transferred to the final formulation. It is already proven that tan δ of rubber compound is basically controlled by inter-aggregate distance between filler particles [30]. As the CA has the potential to disperse CB in absence of ZnO, so it is also evident from the test results that the lowering of tan δ is mainly because of CA activity. While ZnO was used in the master stage, there were not many changes observed in tan δ. Still there is an increment of E' value. The presence of reactive ZnO leads to formation sorter sulfur crosslink and results in higher E' value.

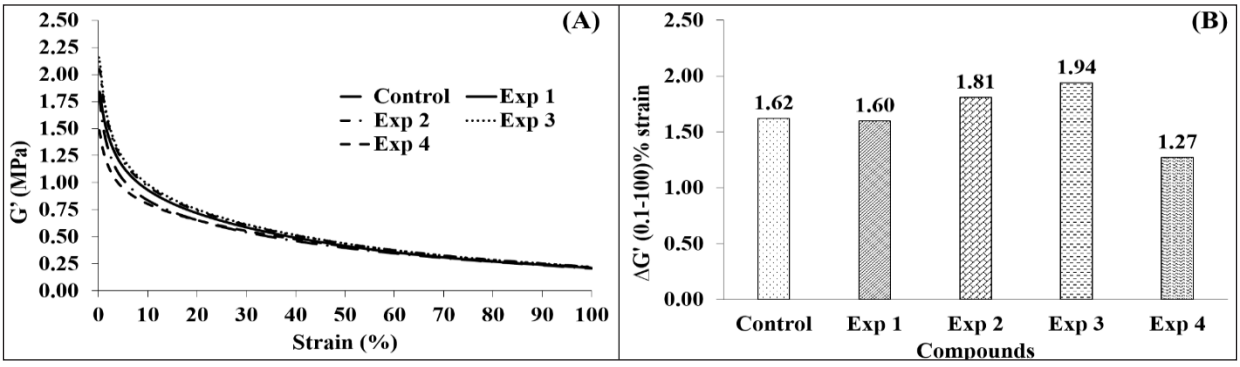

Figure 5. (A) Graphical representation of Payne Effect, (B) Payne effect represent by Bar Chart.

Table 5. Dynamic mechanical properties.

DMA at 5% strain,11 Hz					
DMA at 30 °C	Control	Exp 1	Exp 2	Exp 3	Exp 4
E' (MPa)	7.25	7.51	7.89	7.68	6.5
E" (MPa)	1.27	1.30	1.43	1.35	0.93
tan delta (tan δ)	0.175	0.173	0.181	0.175	0.143
DMA at 70 °C	Control	Exp 1	Exp 2	Exp 3	Exp 4
E' (MPa)	5.94	6.27	6.50	6.38	5.67
E" (MPa)	0.87	0.93	1.02	0.96	0.69
tan delta (tan δ)	0.147	0.148	0.157	0.151	0.121
DMA at 100 °C	Control	Exp 1	Exp 2	Exp 3	Exp 4
E' (MPa)	4.92	5.28	5.40	5.31	4.89
E" (MPa)	0.65	0.72	0.79	0.74	0.54
tan delta (tan δ)	0.131	0.137	0.146	0.140	0.11

3.8 TEM Images

One of the most important parts of this study is to determine the micro-level dispersion of CB in a natural rubber matrix. TEM is a very useful tool for microscopic analysis to understand the degree of dispersion and orientation of the filler in higher magnification. Microscopic images were captured at 1100× magnification by TEM from the cured slabs and it is represented in Figure 6. From the TEM images, it is seen that for Exp 4 compound, CB is good distributed throughout the rubber matrix. This observation is also correlating with the Payne effect results, i.e. the lowering of ΔG' in Exp 4 compound owing to well dispersion of CB, which is discussed in section 3.6. With addition of ZnO in master formulation (i.e. for Exp 1, Exp 2 and Exp 3 compounds), leads to relatively lower CB dispersion while comprising with Exp 4 compound. Agglomeration of CB is clearly visible in rubber matrix in Exp 1, Exp 2 and Exp 3 compounds.

3.9 LAT100 Results

The abrasion resistance rating of the experimental compound Exp 4 against the control was presented in Table 6. One of the targets of this study is to find out a plausible compound formulation where the compound will have the lowering hysteresis loss with a comparable abrasion loss. Exp 4 compound was chosen against control because of the lower hysteresis value in Exp 4 compound among other variants. As per the average ratings, Exp 4 exhibited a better wear rating (103) than the control (100) compound across severities. This signifies that, CA was not only instrumental in lowering the hysteresis of the compound, but also improved the wear properties. This might be due to the chemical interaction of CA with the surface functional groups present in carbon black as discussed in the mechanism section, thereby, forming the chemical bonds, which are much more stable than the conventional physical bonds that were created during the reinforcement of carbon black compounds. As a consequence of stronger chemical bonds, CA has provided better reinforcement in the experimental compound (Exp 4) as compared to the control. The enhanced wear characteristic of Exp 4 reflected its improved reinforcement.

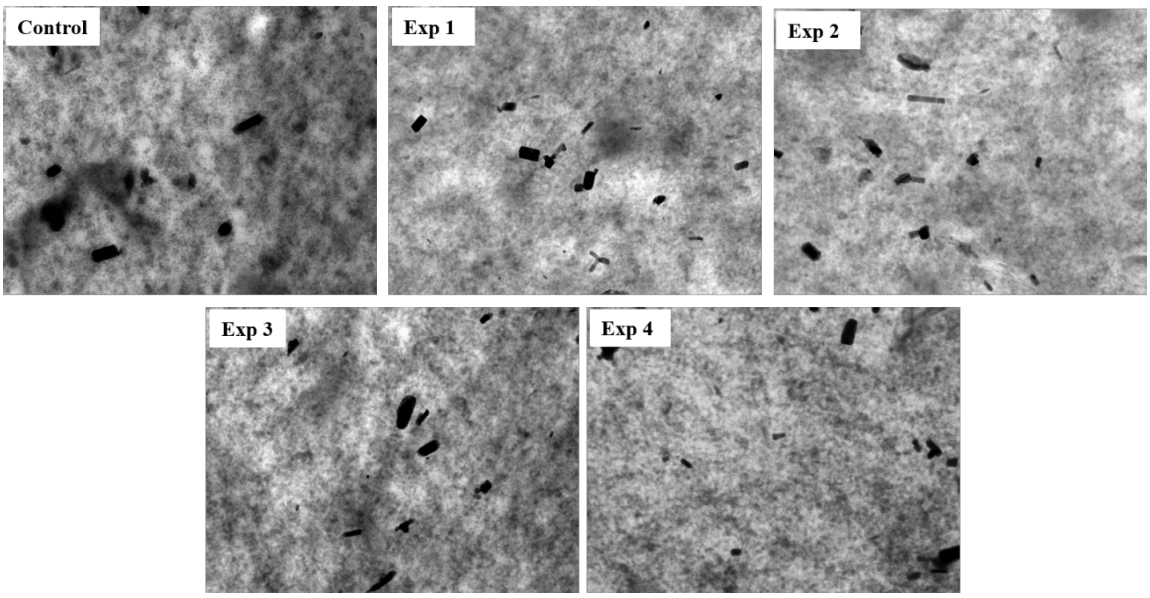

Figure 6. TEM images (comparison at 1100× magnification).

Table 6. LAT 100 test configuration and results.

Abrasion loss test condition			**Wear rating**	
Load (Newton)	Speed (km/ hour)	Slip angle (º)	Control	Exp 4
75	25	16	100	94
		9	100	99
		5.5	100	90
	12	16	100	101
		9	100	113
		5.5	100	111
	2.5	16	100	108
		9	100	97
		5.5	100	112
Average rating*			100	103

*higher the ratings better the abrasion resistance.

4. Conclusions

This study unveils the great potential of the Carbon Black (CB) coupling agent in the natural rubber carbon black system. While ZnO is added to the master formulation, CA acts as an anti-reversion agent and for Exp 3 compound shows a 65% improvement in reversion compared to the control compound. On the other hand, while ZnO fully transferred to the final formulation, Bound rubber (BR) content increased by 19%, the difference in storage modulus (ΔG') is reduced by 22%, CRI improved by 14% and slightly improve in elongation at break compare to control compound. Bound rubber content, Payne effect and microscopic study through TEM have substantiated the potential of the CA on CB dispersity in absence of ZnO from the master formulation. In addition to that hysteresis loss is lowered by 18% with comparable dynamic stiffness (E') at 70 °C compare to the control compound. Abrasion loss was measured to assess the potential of CA in practical application. Abrasion resistance is slightly improved in Exp 4 compound when compared with the control compound. Overall, it was observed that CB CA can act as an anti-reversion agent as well carbon black coupling agent depending on the presence of the ZnO in the compound formulation.

Author Contributions

Koushik Pal: Conceptualization, methodology, compound mixing, data generation, investigation, writing -original drift.

Koushik Banerjee: Compound mixing, compound level testing, data generation, writing - review.

Soumya Ghosh Chowdhury: Formal analysis, investigation, writing - review.

Sanjay Kumar Bhattacharyya: Conceptualization, resources, review and editing supervision.

Rabindra Mukhopadhyay: Conceptualization, resources, review and editing, supervision.

Conflict of Interest

The authors declared no potential conflicts of interest with respect to the research, authorship, and/or publication of this research article.

Acknowledgements

All authors would like to thank "Hari Shankar Singhania Elastomer and Tire Research Institute" management for giving kind permission to publish this research article.

References

[1] Dong, B., Liu, C., Lu, Y., et al., 2016. Effects of hybrid filler networks of carbon nanotubes and carbon black on fracture resistance of styrene-butadiene rubber composites. Polymer Engineering and Science. 56, 1425-1431.
DOI: https://doi.org/https://doi.org/10.1002/pen.24379

[2] Byers, J.T., 2002. Fillers for balancing passenger tire tread properties. Rubber Chemistry and Technology. 75, 527-548.
DOI: https://doi.org/10.5254/1.3547681

[3] Bhawal, P., Das, T.K., Ganguly, S., et al., 2019. Selective cross-linking of carboxylated acrylonitrile butadiene rubber and study of their technological compatibility with poly(ethylene-co-methyl acrlylate) by means of mechanical, thermal, and chemical analysis. Polymer Bulletin. 76, 1877-1897.
DOI: https://doi.org/10.1007/s00289-018-2474-z

[4] Zhang, P., Morris, M., Doshi, D., 2016. Materials development for lowering rolling resistance of tires. Rubber Chemistry and Technology. 89, 79-116.
DOI: https://doi.org/10.5254/rct.16.83805

[5] Das, T.K., Bhawal, P., Ganguly, S., et al., 2019. Synthesis of hydroxyapatite nanorods and its use as a nanoreinforcement block for ethylene methacrylate copolymer matrix. Polymer Bulletin. 76, 3621-3642.
DOI: https://doi.org/10.1007/s00289-018-2565-x

[6] Urreaga, J.M., Matias, M.C., De la Orden, M.U., et al., 2000. Effects of coupling agents on the oxidation and darkening of cellulosic materials used as reinforcements for thermoplastic matrices in composites. Polymer Engineering and Science. 40, 407-417.

DOI: https://doi.org/10.1002/pen.11174

[7] Hess, W.M., Klamp, W.R., 1983. Effects of carbon black and other compounding variables on tire rolling resistance and traction. Rubber Chemistry and Technology. 56, 390-417.
DOI: https://doi.org/10.5254/1.3538134

[8] Hall, D.E., Moreland, J.C., 2001. Fundamentals of rolling resistance. Rubber Chemistry and Technology. 74, 525-539.
DOI: https://doi.org/10.5254/1.3547650

[9] Bhattacharya, A.B., Pandy, M., Naskar, K., 2021. Development of NR/SBR based rubber compounds with low hysteresis and high durability for transmission v-belts applications. Organic Polymer Material Research. 3, 5.
DOI: https://doi.org/10.30564/opmr.v3i1.3568

[10] Das, T.K., Ghosh, P., Das, N.C., 2019. Preparation, development, outcomes, and application versatility of carbon fiber-based polymer composites: a review. Advanced Composite and Hybrid Material. 2, 214-233.
DOI: https://doi.org/10.1007/s42114-018-0072-z

[11] Pandey, J.K., Singh, R.P., 2005. Green nanocomposites from renewable resources: Effect of plasticizer on the structure and material properties of clay-filled starch. Starch/Staerke. 57, 8-15.
DOI: https://doi.org/10.1002/star.200400313

[12] Zafarmehrabian, R., Gangali, S.T., Ghoreishy, M.H.R., et al., 2012. The effects of silica/carbon black ratio on the dynamic properties of the tread compounds in truck tires. E-Journal of Chemistry. 9, 1102-1112.
DOI: https://doi.org/10.1155/2012/571957

[13] Khodabakhshi, S., Fulvio, P.F., Andreoli, E., 2020. Carbon black reborn: Structure and chemistry for renewable energy harnessing. Carbon. 162, 604-649.
DOI: https://doi.org/10.1016/j.carbon.2020.02.058

[14] Choi, S.S., Kim, J.C., Ko, J.E., et al., 2007. Influence of coupling agent on properties of carbon black-reinforced SBR and NR/SBR vulcanizates. Journal of Industrial and Engineering Chemistry. 13, 1017-1022.

[15] Sattayanurak, S., Sahakaro, K., Kaewsakul, W., et al., 2020. Synergistic effect by high specific surface area carbon black as secondary filler in silica reinforced natural rubber tire tread compounds. Polymer Testing. 81, 106173.
DOI: https://doi.org/10.1016/j.polymertesting.2019.106173

[16] Chowdhury, S.G., Pal, K., Satpathi, H., et al., 2020. Improving hysteresis of a typical carbon black-filled natural rubber tread compound by using a novel coupling agent. Progress in Rubber, Plastic and Recycling Technology. 36, 245-261.
DOI: https://doi.org/10.1177/1477760619895015

[17] González, L., Rodríguez, A., de Benito, J.L., et al., 1996. A new carbon black-rubber coupling agent to improve wet grip and rolling resistance of tires. Rubber Chemistry and Technology. 69, 266-272.
DOI: https://doi.org/10.5254/1.3538371

[18] Stoček, R., Kratina, O., Ghosh, P., et al., 2017. Influence of thermal ageing process on the crack propagation of rubber used for tire application. Springer Series in Materials Science. 247, 351-364.
DOI: https://doi.org/10.1007/978-3-319-41879-7_24

[19] Jitkarnka, S., Chusaksri, B., Supaphol, P., et al., 2007. Influences of thermal aging on properties and pyrolysis products of tire tread compound. Journal of Analytical and Applied Pyrolysis. 80, 269-276.
DOI: https://doi.org/10.1016/j.jaap.2006.07.008

[20] Choi, S.S., 2006. Influence of polymer-filler interactions on retraction behaviors of natural rubber vulcanizates reinforced with silica and carbon black. Journal of Applied Polymer Science. 99, 691-696.
DOI: https://doi.org/10.1002/app.22562

[21] Han, S., Kim, W.S., Mun, D.Y., et al., 2020. Effect of coupling agents on the vulcanizate structure of carbon black filled natural rubber. Composite Interfaces. 27, 355-370.
DOI: https://doi.org/10.1080/09276440.2019.1637197

[22] Qian, S., Huang, J., Guo, W., et al., 2007. Investigation of carbon black network in natural rubber with different bound rubber contents. Journal of Macromolecular Science, Part B Physics. 46(B), 453-466.
DOI: https://doi.org/10.1080/00222340701257588

[23] Wolff, S., Wang, M.J., Tan, E.H., 1993. Filler-elastomer interactions. Part VII. Study on bound rubber. Rubber Chemistry and Technology. 66, 163-177.
DOI: https://doi.org/10.5254/1.3538304

[24] Kilinçarslan, Ş., Türker, Y.Ş., 2020. Investigation of wooden beam behaviors reinforced with fiber reinforced polymers. Organic Polymer Material Research. 2, 1-7.
DOI: https://doi.org/10.30564/opmr.v2i1.1783

[25] Maurya, S.D., Singh, M.K., Amanulla, S., et al., 2022. Mechanical, electrical and thermal properties of nylon-66/flyash composites: Effect of flyash. Organic Polymer Material Research. 4, 7-14.
DOI: https://doi.org/10.30564/opmr.v4i2.5233

[26] Huang, S.T., Duh, Y.S., Hsieh, T.Y., et al., 2012. Thermal analysis for nano powders of iron and zinc by DSC. Procedia Engineering. 45, 518-522.
DOI: https://doi.org/10.1016/j.proeng.2012.08.196

[27] Milani, G., Milani, F., 2012. Comprehensive numerical model for the interpretation of cross-linking with peroxides and sulfur: Chemical mechanisms and optimalvulcanization of real items. Rubber Chemistry and Technology. 85, 590-628.
DOI: https://doi.org/10.5254/rct.12.88945

[28] Hassan, M.M., Wagner, M.H., Hayder, U., 2012. Study on the performance of hybrid jute / betel nut fiber reinforced polypropylene composites. Journal of Adhesive Science and Technology. 25, 615-626.
DOI: https://doi.org/10.1163/016942410X525858

[29] Hassan, M.M., Wagner, M.H., Zaman, H.U., et al., 2010. Physico-mechanical performance of hybrid betel nut (Areca catechu) short fiber/seaweed polypropylene composite. Journal of Natural Fibers. 7, 165-177.
DOI: https://doi.org/10.1080/15440478.2010.504394

[30] Pal, K., Chowdhury, S.G., Mondal, D., et al., 2021. Impact of α-cellulose as a green filler on physico-mechanical properties of a solution grade styrene-butadiene rubber based tire-tread compound. Polymer Engineering and Science. 61, 3017-3028.
DOI: https://doi.org/10.1002/pen.25814

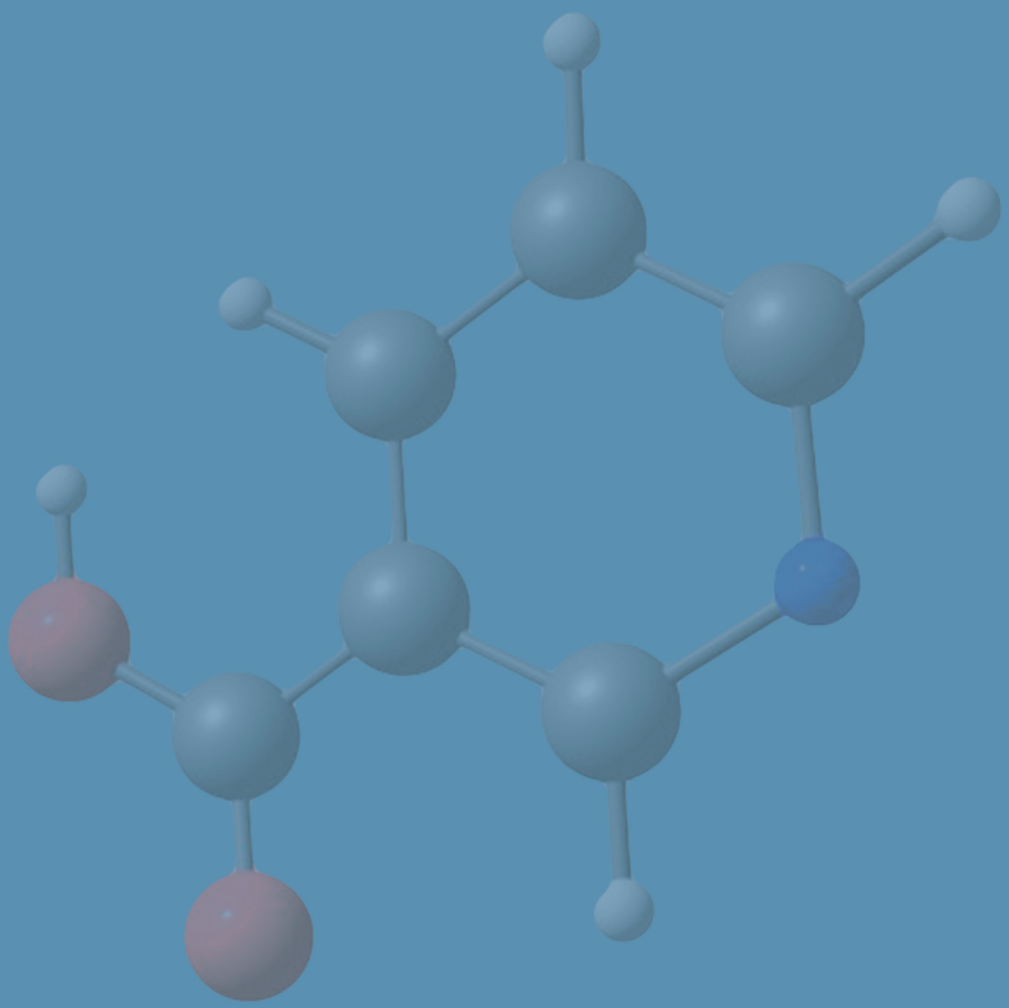

BILINGUAL
PUBLISHING CO.
Pioneer of Global Academics Since 1984

Tel:+65 65881289
E-mail: contact@bilpublishing.com
Website:ojs.bilpublishing.com

2661-3875
02
9 772661 387226